

Title: Hidden patterns of biodiversity loss as birds respond to sea level rise

Abstract: Coastal biodiversity is being reshaped by sea-level rise (SLR). Most efforts to anticipate these changes focus on species counts or range shifts, yet these changes often alter ecosystem functions. We combined a probabilistic AI hurdle model and a trait-based analysis to examine the impact of SLR on birds across the coastal Gulf of Mexico, and how those changes affect functional diversity within three trait groups—namely, movement, foraging, and social behavior. We found that SLR would reduce coastal ecosystem resilience and cause biodiversity loss across multiple angles, including functional richness, redundancy, evenness, and divergence. Surprisingly, the most impacted areas are not the exposed shoreline, but instead are landward coastal transition zones. Furthermore, avian biodiversity is maintained or expanded in coastal protected areas. These reserves, therefore, function as refugia embedded in a surrounding landscape where unique combinations of species traits are lost. Climate-adaptive actions should secure landward migration corridors and tidal channels, and manage reserve productivity to avoid irreplaceable biodiversity loss.

Main Text:

Global environmental change and human activities pose mounting threats to biological diversity (Olden et al., 2008). Birds exemplify the consequences of these threats: habitat loss and degradation, fisheries bycatch (for seabirds), pollution, prey depletion, and climate variability have driven widespread population declines and eroded functional diversity in birds (Dias et al., 2019; Rosenberg et al., 2019; Saintilan et al., 2014). Superimposed on these drivers, sea-level rise (SLR) is rapidly altering coastal geomorphology and flooding regimes, with the IPCC and U.S. federal assessments projecting substantial increases in chronic high-tide flooding and storm-driven extremes on multi-decadal horizons, thereby compressing (“squeezing”) intertidal habitats critical to coastal birds (NOAA, 2022).

Tidal-marsh specialists experience more frequent spring-tide nest inundation and lowered productivity—well documented for Saltmarsh Sparrow, where flooding is common even today and expected to worsen with accelerating SLR (Bayard & Elphick, 2011; Cook et al., 2024). Beach-nesting shorebirds (e.g., Piping Plover) face direct loss and fragmentation of supratidal nesting habitats and higher probabilities of storm-surge overwash. Projections for barrier-island systems show substantial declines in suitable breeding areas under SLR scenarios, even as post-storm sediment dynamics can occasionally create transient habitat patches (Seavey et al., 2011). Migratory shorebirds also risk diminished carrying capacity at stopover sites as intertidal foraging flats drown or are pinched against hardened shorelines, reducing roosting options and energetic refueling opportunities (Galbraith et al., 2005). For seabirds on low-lying oceanic islands, SLR combined with storm waves and groundwater rise elevates overwash risk, nest failure, and colony displacement, highlighting the need for higher-elevation refugia and assisted colonization in some archipelagos (Reynolds et al., 2015). Together, these processes indicate that avian population declines increasingly translate into functional erosion (Adams et al., 2025) via the selective loss of flood-sensitive foraging and breeding strategies—underscoring the need for trait-explicit analyses embedded in standardized frameworks to forecast ecosystem consequences and guide adaptation (Intergovernmental Panel on Climate Change (IPCC), 2023).

Species distribution models (SDMs) provide a practical framework for interpolating species’ distributions across space and time from occurrence and/or abundance records (Botella et al., 2018), enabling the estimation of biodiversity metrics and scenario-based forecasting of environmental or anthropogenic change (Elith & Leathwick, 2009; Pearson & Dawson, 2003). Recent advances in machine learning and deep learning have improved predictive performance by capturing non-linear responses and spatial structure and by integrating heterogeneous data sources (e.g., remote sensing, environmental covariates, citizen-science observations) (Adadi, 2021). Artificial intelligence-driven species distribution models have attracted attention for their practical utility for conservation planning, risk assessment, and ecological forecasting. For example, Lee et al. (2022) predicted the spread of invasive species under climate change, Ennakri et al. (2025) presented how AI SDMs support biodiversity monitoring at scale, and Ryo et al. (2020) informed conservation decision-making through interpretable and ecologically grounded models. The superior predictive accuracy of artificial intelligence to capture complex, non-linear relationships and spatial patterns leads to improved accuracy, especially for less-represented species (Botella et al., 2018). Transfer learning and foundation-model approaches further extend SDMs to data-sparse species via few-shot and zero-shot inference (Dinnage, 2024). Generative and masked-autoencoder strategies have yielded high discrimination and calibration across diverse taxa and large occurrence datasets (Yan et al., 2024).

Despite these advances, significant gaps remain. Existing deep-learning SDMs disproportionately focus on species occurrence. Modeling species abundance is rarely explored in deep learning, which restricts our understanding of demographic changes in species in response to environmental and anthropogenic changes (Thuiller et al., 2004). More importantly, most progress in community ecology has been made in quantifying species numbers (taxonomic units) as correlates of functional diversity or biodiversity, while neglecting that species’ functional traits are actual representations of ecosystem functions and can differ within the same species. Additionally, species distribution models pipelines decouple species’ environmental envelopes and species replacement or co-occurrence relations, even though both operate jointly in nature as species niches. Thus, they are poorly suited to forecast how environmental change reshapes communities and biodiversity (McGill et al., 2006).

Addressing these gaps requires a unified architecture that synthesizes environmental drivers and interspecific relations, as well as the abundance and functional diversity of species and communities. A functional trait diversity perspective to community ecology can discover how ecosystem functions of communities vary along environmental gradients (Violle et al., 2007) (such as landscapes changed by sea level rise scenarios shown in this study). Functional traits are morphological, physiological, or behavioral characteristics of organisms that can be quantified at various organizational levels, ranging from individuals to ecosystems. Species resiliencies are related to functional traits. With changes in habitat, species with poorly adapted traits are likely to disappear. In communities where redundancy is low—or where functionally unique species are lost—ecosystem functioning can decline disproportionately (Biggs et al., 2020; Violle et al., 2017).

This study introduces a generative probabilistic AI hurdle model framework to predict 350 bird species abundance across the Northern Gulf of America, formerly known as the Gulf of Mexico. Based on the deep learning

model prediction, an abundance-weighted trait probability analysis was conducted to address the gaps in quantifying environmental change-driven biodiversity change based on species ecosystem functions. We (i) modeled species–species dependence alongside spatial–temporal co-occurrence in shared environment; (ii) adopted a hurdle likelihood to handle zero inflated species observation data by modeling occurrence (Bernoulli–logit) and positive abundance conditional on presence (e.g., Poisson or Negative Binomial) separately (Edmondson et al., 2021); and (iii) integrated species trait information to connect niches, traits, and ecosystem functions with environmental change (sea level rises and ecosystem productivity change with SLR). Applied across different habitat bird species, our approach yields spatially explicit forecasts of species expected abundance and trait-based biodiversity change under SLR. Surprisingly, we found that the most significant biodiversity loss occurred in the landward lower uplands rather than the exposed shoreline from SLR. Fine-scale patterns of biodiversity changes were mapped to guide conservation and reserve operations to avoid irreversible biodiversity loss due to sea level rise.

AI extended abundance prediction beyond observing efforts.

Limited observing efforts confined by resources supporting ecosystem monitoring have significantly constrained our ability to define long-term and large-scale ecosystem and biodiversity patterns, especially at the species level. A location at a period of time that lacks strategic observation is not identical to a lack of biodiversity; however, if we quantify biodiversity based on biased observation, we will have a biased view of biodiversity. Figure 1 showed us that if we make abundance prediction only within areas where species were spotted, we may misinterpret species range and unobserved patterns, as shown by the generative AI zero-shot predicted expected abundance. The AI hurdle model can still predict 0 count of species even when we attempt to let it predict across the whole study area (shown in the AI zero-shot prediction for Black-bellied Whistling Duck). Coastal species, such as Osprey, are still present within their coastal range, although we construct the prediction cover spanning a range of habitats from woodlands to marshes. For grassland birds such as the Brown Thrasher, the limited inland observations mean that abundance is often predicted solely from species presence or observation, and delicate inland range patterns will not be revealed. As we found in AI zero-shot prediction, Brown Thrasher's range extends into inland waters and channels based on interspecific relations (Figure 2) and the environmental niches of species (Supplementary Information Figure 4). On the ridge of the mountains or in the middle of the deep water, where it is possible to spread a web of observers, AI can determine the suitability of habitats for species based on learned patterns from observation data and fill the gaps in observation, as it does in the river channel in Oklahoma in American Goldfinch observation.

Because of AI models' capacity to capture non-linearities in ecosystem interactions and processes, the models we presented here achieve a high average predictive performance for abundance (RMSE) of 0.68 regardless of the number of observations per species. And the occurrence prediction performance (F1 score) of 0.86 for species with at least 0.1 prevalence. The best species distribution model performance in Norberg et al. (2019) is 0.4. We reported the distribution of (F1 score (classification performances, RMSE (regression performance) of individual species models, and confusion matrices by species/habitat in Supplementary Materials Fig. 4.

Using this AI model's capabilities, we could project species range and abundance distributions under sea-level rise, with modified coastal inundation levels and marsh migration trajectories. Species abundance distribution map of scenarios with and without sea level rise is provided in the supplementary information table 1. The scenario maps showed persistence clustering along tidal creek networks and near estuary mouths, while back-barrier/impounded locations lose suitability—i.e., places with better tidal exchange fare better. The hotspot of species distribution geography shows very different pictures with SLR compared to scenarios without SLR. Some species become more fragmented as a result of adaptation to sea level rise, such as the Great Egret, Brown Pelican, and the Ring-billed Gull. The American Crow and House Sparrow are generalists that display the largest scenario deltas; however, a contraction near the coast and a shift up-estuary were observed. Forest birds, such as house finch and Red-bellied Woodpecker, show a modest coastal retreat but retain strong interior holdouts.

The AI Hurdle model learns both the interspecific associations among birds (Fig. 2) and their environmental niches (Supplementary Fig. 4). The neural network ingests 28 environmental and observation covariates, leveraging their spatial structure and cross-correlations, and maps these predictors to species distributions. To capture local, nonlinear species–environment relationships, the model uses a probabilistic latent-variable layer with a Gaussian prior. Across the study, this induces approximately 5.4 million latent variables that support abundance predictions for 350 species. From these learned latent codes, the associated species embeddings (i.e., vectors that position species in the shared latent space), were derived and we used these species vector (2048 long for each species) to present interspecific relation structure that the model has learned and visualize it as ordered correlation/interaction heat maps (Figure. 2) and species-by-feature response patterns (Supplementary Fig. 4). Species are closest to each other in the heat maps if their embedding vector have strongest correlation than what they have with other species. Therefore, in the latent species, species were positioned based on their environmental niche and positions in the trophic niche. Zooming in on

the top-left corner, we saw species either from woodlands or scrubs. In the bottom right, species long to ocean and coastal species groups. We also found that the terrestrial species in the top-left corners tend to have a negative correlation with each other's population, and the bottom-right species have a positive correlation with each other's population.

5

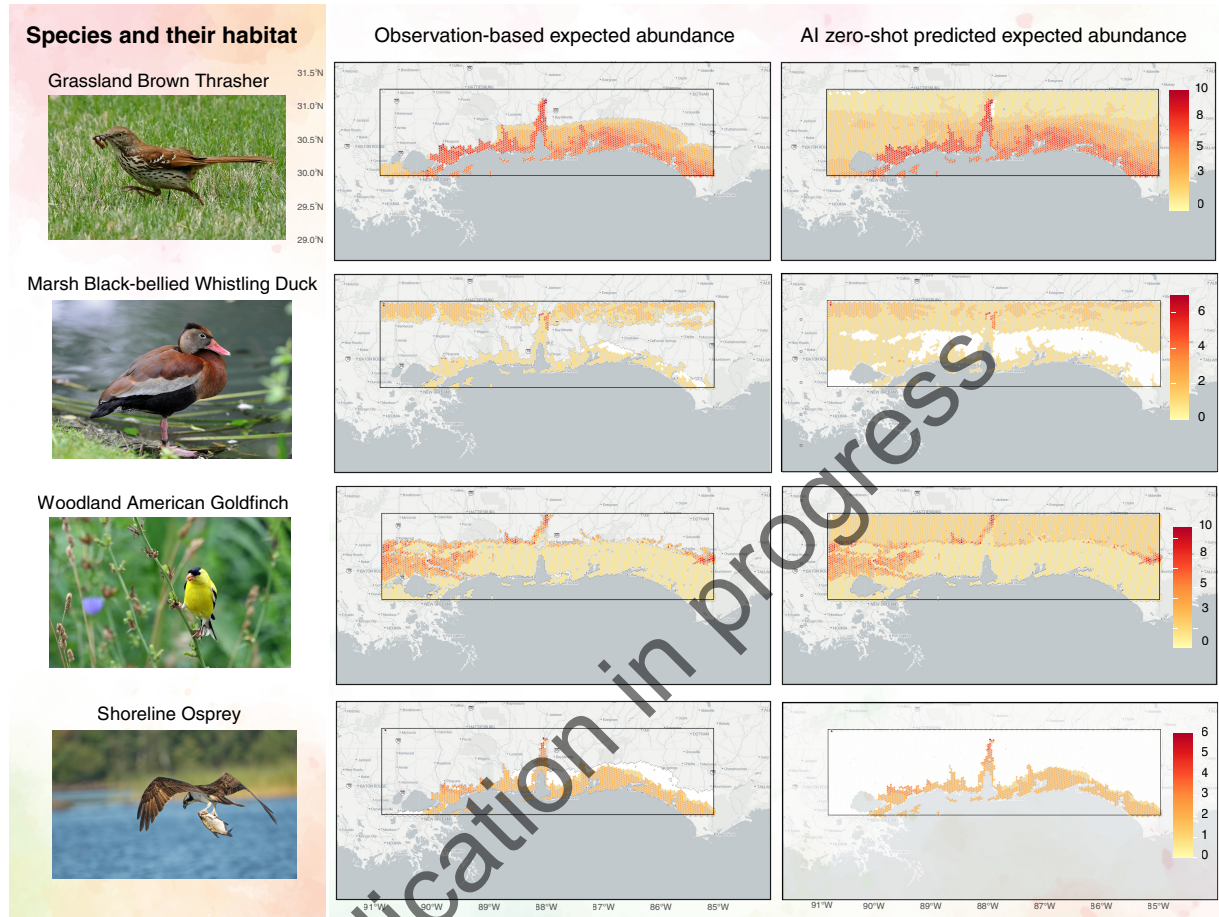


Figure 1. Observation-based species expected abundance and AI zero-shot (generative) predicted species abundance of examples of birds in four different habitats, namely Brown Thrasher in grassland, Black-bellied Whistling Duck, American Goldfinch in Woodland, and Osprey in shoreline habitat. The rectangular frames in the middle of the maps are the modeling areas. The color scales represent predicted counts of focal species at that location. Count values are expected abundance because the abundance of each location is calculated by multiplying the stochastically predicted occurrence probability and predicted counts if the species is present. White pixels mean that the location was predicted to have zero population. Transparent through base map indicates no predicted value or out of the study area.

10

15

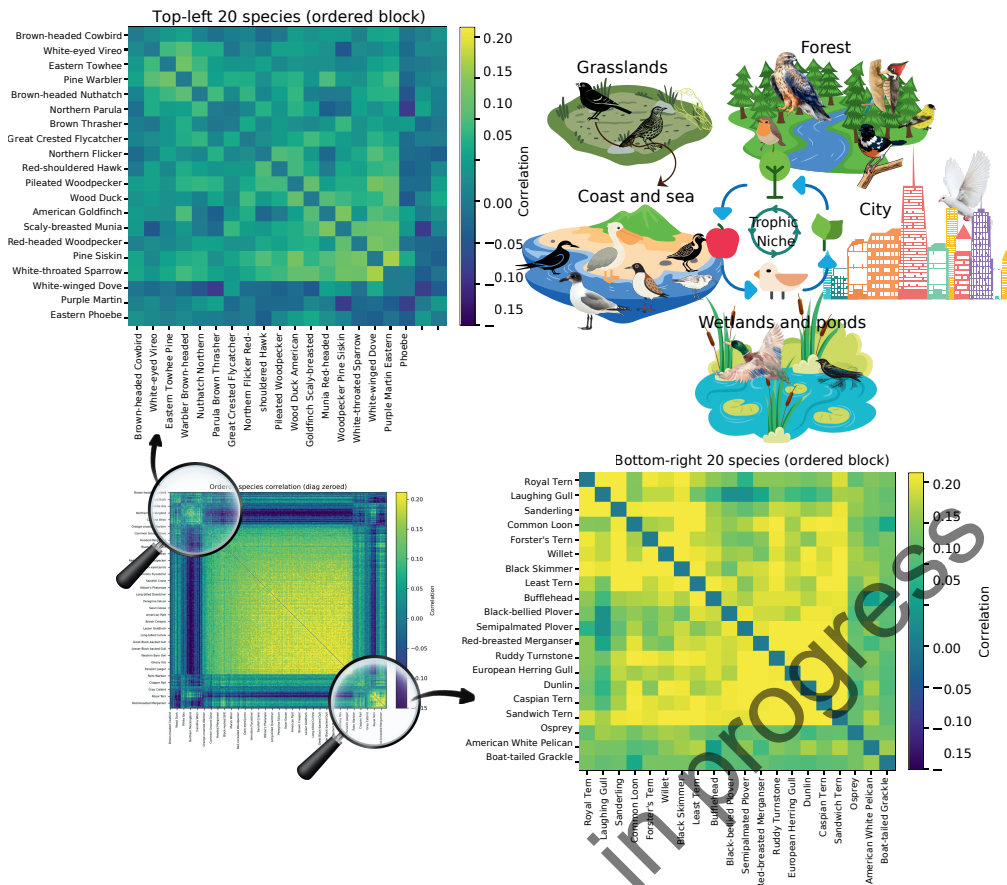


Figure 2. Species relation matrix reveals species co-occurrence and replacement relations in habitats. Each cell shows the pairwise correlation between the learned embedding vectors of species i and j (2048 positioning vector in the species embeddings from the AI hurdle model). Values range from -1 to +1 and are displayed with a diverging color scale centered at 0: warm colors (toward red) indicate positive association (species occupy similar positions in the embedding space and tend to co-occur or share environmental responses); cool colors (toward blue) indicate negative association (replacement responses).

Uncovering the hidden patterns of biodiversity loss

Through abundance-weighted trait analysis, we found that local functional richness is, historically, highest in a narrow coastal ribbon that tracks the Mississippi Sound barrier-island chain (Cat, Ship, Horn, Petit Bois–Dauphin Island), the Grand Bay marsh complex, and the Mobile Bay–Tensaw Delta. Eastward, elevated values continue along back-barrier and estuarine shorelines of Perdido–Pensacola Bay, Santa Rosa Sound, and Choctawhatchee Bay (Figure 3). These hotspots coincide with shallow, structurally diverse wetland mosaics that host many flight-strategy and dispersal types (e.g., strong fliers, short-hop residents, wide-ranging coastal movers). Richness falls off both offshore (open Gulf cells south of the islands) and inland (toward the northern edge of the frame), both of which lack the fine-grained wetland complexity that supports diverse assemblages. These areas occupy the cooler color bins on the historical map (roughly the 30–40 range for movement trait richness).

Under SLR, the overall palette shifts cooler. Coastal cells closest to the shoreline show localized increases in functional richness while maintaining steady redundancy. These gains likely reflect short-range redistribution into newly wetted edge habitats and the persistence of tidal corridors that continue to support diverse movement modes. The largest richness declines form a coast-parallel band inland of the shoreline — roughly between the back-barrier edge and lower uplands (−20% to −40% in the percentage change panel). Hotspots persist most clearly in sheltered bay areas and a few back-barrier reaches, but they are narrower and less intense than historically, reflecting the loss of low-elevation marsh and supratidal habitats that supported a wide spread of movement strategies. Moving slightly inland and uplands, changes are modestly negative. In short, SLR drives coastal thinning and segmentation of movement functional richness.

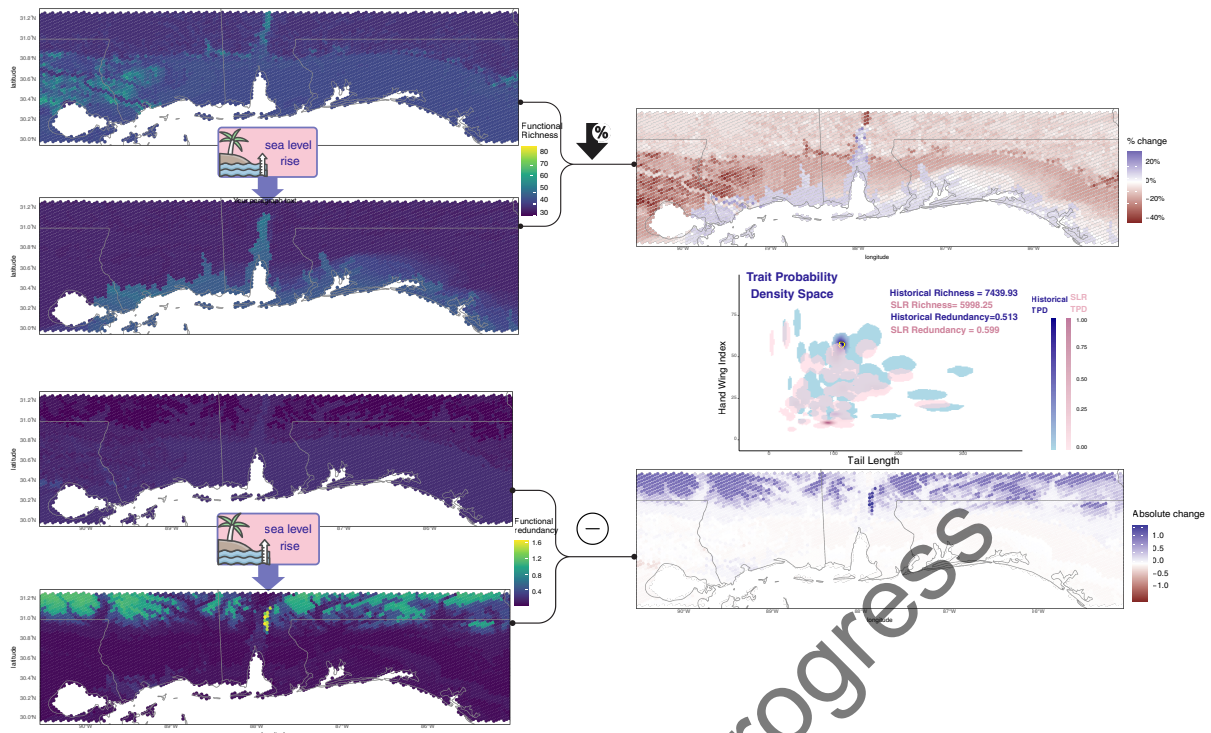


Figure 3. Abundance-weighted functional richness and redundancy of 350 species movement traits with and without sea level rise impacts, and their changes with sea level rises, accompanied by trait probabilistic hypervolumes (density probability of the full range of species traits combination). Color scales represent either trait diversity index values or trait diversity change values, the Hand Wing Index, and the Tail Length composite movement trait space. If the trait index values are pretty small, we use the absolute change value to prevent extremely large change values

High redundancy means ecosystems can absorb species losses while still maintaining key functions. Functional redundancy is highest along the same coastal mosaic where habitats and resources are broad and repeated—Mississippi Sound’s marsh–barrier system (Cat/Ship/Horn/Petit Bois–Dauphin Island), the Mobile Bay–Tensaw Delta complex, and the western Florida Panhandle embayments from Perdido–Pensacola through Santa Rosa and Choctawhatchee—reflecting multiple species filling similar roles within productive, shallow estuarine settings with SLR. Redundancy is comparatively lower offshore (open-water Gulf cells) and in inland/upland cells where fewer species co-occur and trait overlap is limited (Figure 4). Under the sea-level-rise scenario, Movement functional redundancy is relatively stable along the immediate coast, remaining moderate through much of the barrier-island/estuarine corridor. By contrast, a broad inland/back-barrier belt exhibits a marked increase in redundancy. From a regional standpoint, redundancy increases slightly overall (from 0.513 to 0.599), meaning regional trait assemblages become more compositionally concentrated as shorelines retreat.

The contracting richness and rising redundancy inland prove functional homogenization and biodiversity loss with SLR. Surprisingly, redundancy increases most significantly in uplands, meaning upland species loss is in a smaller number of species but with distinctive movement strategies lost, and the remaining species cluster into overlapping roles. The directly exposed coastal cells didn’t see either a decrease in richness or an increase in redundancy. While even where inland richness losses are modest, the sharp redundancy gains signal reduced ecosystem versatility and lower resilience to additional stressors (e.g., storms, heat waves, prey shifts), as fewer complementary movement modes remain to sustain processes when conditions change.

These results suggest a shift from diverse, complementary coastal assemblages to more redundant inland assemblages under SLR from a regional perspective. Management actions that conserve or restore trait-diverse coastal wetland mosaics (e.g., living shorelines, sediment/nourishment to maintain back-barrier marsh platforms, protection of estuarine corridors) should help retain movement strategy breadth where it is currently highest, while efforts inland should prioritize maintaining complementarity (not just species counts) to avoid further erosion of functional versatility.

Functional evenness and divergence are two distinct components of functional diversity. In Figure 3, functional evenness represents the uniformity of species abundance across occupied trait space; high values indicate similar contributions of variety strategies, whereas low values indicate dominance by a few strategies and gaps in trait use. In contrast, functional divergence measures how far species with high abundances at a location are from the center of the community's functional space, with a higher value indicating the prevalence of extreme traits. In terms of resiliency, high divergence may indicate communities that provide unique functions, but that are fragile if species disappear. A community where traits are evenly represented is more resilient to environmental fluctuations.

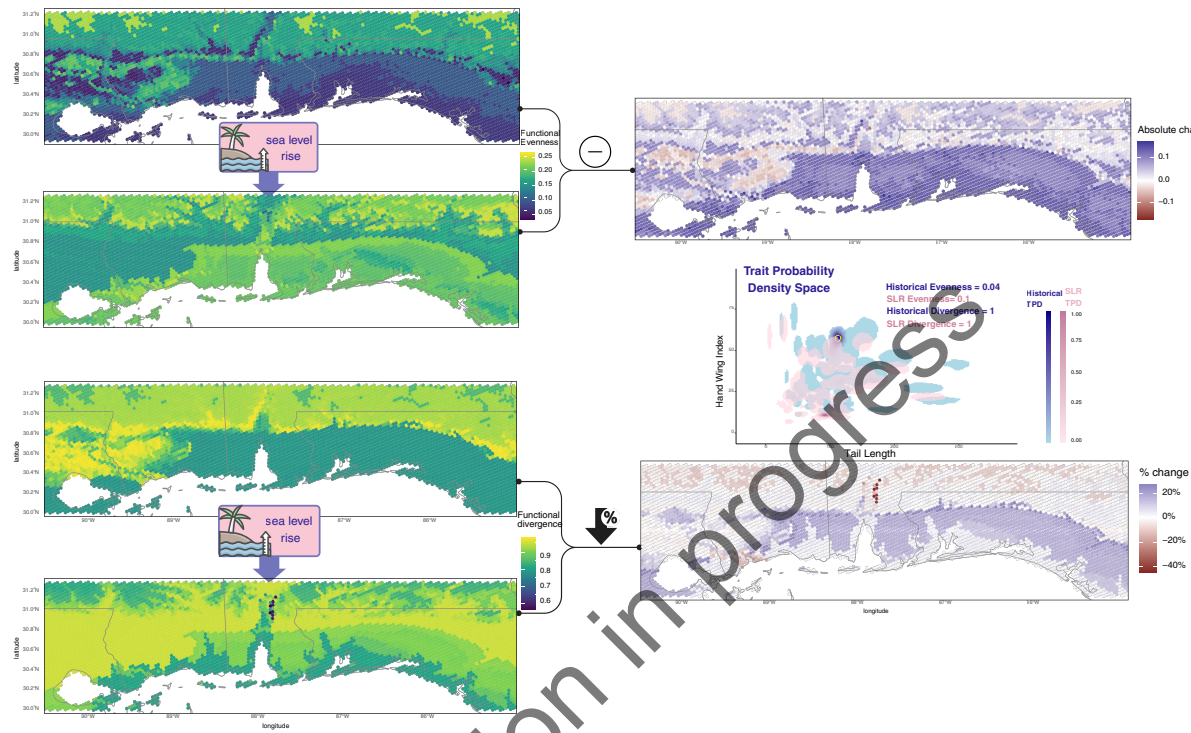


Figure 4. Abundance-weighted functional evenness and divergence of 350 species movement traits (Hand wing index and tail length) with and without sea level rise impacts, and their changes with sea level rises, accompanied by trait probabilistic hypervolumes (density probability of the full range of species traits combinations). Color scales represent either trait diversity index values or trait diversity change values, the Hand Wing Index, and the Tail Length composite movement trait space. If the trait index values are pretty small, we use the absolute change value to prevent extremely large changes.

Evenness is spatially structured and shifted into a fragmented pattern under sea-level rise (SLR). Historically, Evenness is lowest along the immediate coast (dark tones ≈ 0.05 – 0.10), especially around the Mississippi Sound barrier-island rim and the margins of Mobile Bay and the western Florida Panhandle embayments. These cells are dominated by a few movement strategies (e.g., shoreline specialists), yielding an uneven, spread functional trait space (in the trait density space). Higher evenness (≈ 0.15 – 0.25) appears in more interior cells, where assemblages contain a more balanced mix of movement types.

Under the SLR scenario, evenness increased broadly and became more spatially continuous. The shoreline corridor—previously the lowest-evenness zone—shifts into greener/yellower classes (≈ 0.15 – 0.25), indicating reduced dominance by a few coastal strategies. A coast-parallel inland/back-barrier band shows modest but widespread gains in evenness, while the interior/upland belt achieves the smoothest inland trait gradient. The largest increases in functional evenness occur along the Mississippi Sound corridor, spanning Bay St. Louis–Biloxi–Pascagoula and the Grand Bay marsh complex, and extending across the Cat–Ship–Horn–Petit Bois–Dauphin barrier-island chain.

The absolute-change map confirms that SLR flattens the distribution of movement strategies across space (from 0.04 to 0.1) and the removal of rare functional traits: evenness rises almost everywhere, with the shoreline catching up but still lagging inland, consistent with a regional trend toward more uniform use of trait space uplands. This indicates markedly more even partitioning of movement functions among the species that adapted to SLR.

Historical pattern of functional divergence is highest inland and along the back-barrier/northern tier (yellow, $\approx 0.85\text{--}0.90$), and lower along the immediate shoreline and open Gulf cells (teal, $\approx 0.70\text{--}0.80$). The strongest inland values form an arc from coastal Mississippi into Alabama and the western Florida Panhandle, while coastal margins of Mississippi Sound, Mobile Bay, and the Perdido–Pensacola / Santa Rosa–Choctawhatchee shorelines remain comparatively lower. Under SLR, functional divergence shifts seaward: a coast-parallel belt from Mississippi Sound through Mobile Bay to the western Florida embayments increases into the higher classes, producing a more continuous yellow swath along the back-barrier/shoreline corridor. Conversely, the interior/upland band shows declines (cooler greens/teals). The percentage change map confirms the widespread positive changes (blue, up to $\approx +20\%$) hugging the coast and negative changes (brown, often -20% to -40%) inland, with a localized decrease hotspot north of Mobile Bay.

SLR favors edge-weighted (extreme trait values), more extreme movement strategies in cells near the coast (rising functional divergence), while inland assemblages become more center-weighted (falling divergence), consistent with the inland increases in redundancy and evenness that were observed. In practical terms, coastal communities trend toward specialization at trait extremes, whereas inland communities flatten toward more generalist mixes as habitats reorganize with SLR.

Peeking inside the space of species' ecosystem functions

We quantified community-level trait-based metrics and generated figures of trait hypervolumes: richness (volume of hypervolumes), redundancy (overlap/backup among similar trait combinations), evenness (balance of use across the occupied space of the hypervolume), and divergence (edge- vs center-weighted use). The whole-region-scale community's realized functional hypervolume—the portion of trait space occupied by species and their abundances—was presented in Figure 5. We found trait richness contracts under SLR, indicating loss of unique combinations, while evenness generally increases, i.e., the combinations that remain are used more uniformly. The directions of change in redundancy and divergence differ by trait group, revealing how the contraction unfolds.

The movement hypervolume shrinks (richness $7,439.93 \rightarrow 5,998.25$), while redundancy rises ($0.513 \rightarrow 0.599$) and evenness increases ($0.04 \rightarrow 0.10$). Divergence stays high ($\approx 1 \rightarrow 1$), implying that, despite volume loss, occupancy continues to weight the edges of movement space—extreme movement strategies persist—but with greater local overlap and a more even spread among those survivors.

The foraging hypervolume also contracts (richness $1,852.58 \rightarrow 1,548.79$), but here redundancy declines sharply ($0.616 \rightarrow 0.328$), evenness rises ($0.08 \rightarrow 0.21$), and divergence increases ($0.60 \rightarrow 0.88$). Together, these shifts indicate pruning of intermediate strategies and a shift toward the edges of foraging space (e.g., more extreme bill/foraging morphologies), with less backup among similar strategies. The system becomes leaner and more specialized, not merely more overlapped.

Social behavior hypervolume shows a modest richness decline ($140.35 \rightarrow 129$), a large drop in redundancy ($4.006 \rightarrow 2.529$), a marked rise in evenness ($0.08 \rightarrow 0.22$), and a decline in divergence ($0.92 \rightarrow 0.84$). Abundance thus shifts toward the center of social-behavior space (fewer extreme social strategies), with less overlap/backup among similar social types but **more** even contributions of those that persist.

These complementary responses help reconcile spatial maps where richness declines while evenness (and sometimes redundancy) increases. Functionally, the community retains some extreme movement types, becomes more specialized in foraging, and less polarized in social strategies—all while overall trait breadth narrows. Management should therefore (i) protect trait-diverse coastal mosaics to maintain movement strategy breadth where it remains highest, (ii) buffer against foraging specialization risk by conserving prey/habitat diversity and cross-habitat linkages (given falling foraging redundancy), and (iii) sustain social-strategy complementarity (colonial vs solitary, territorial vs non-territorial) to avoid further center-ward collapse. Because redundancy changes are trait-group-specific—rising for movement but falling for foraging and social traits—resilience will depend on which functions are targeted: coastal connectivity may still be buffered by movement overlap, whereas trophic and social processes could be more fragile under continued sea-level rise.

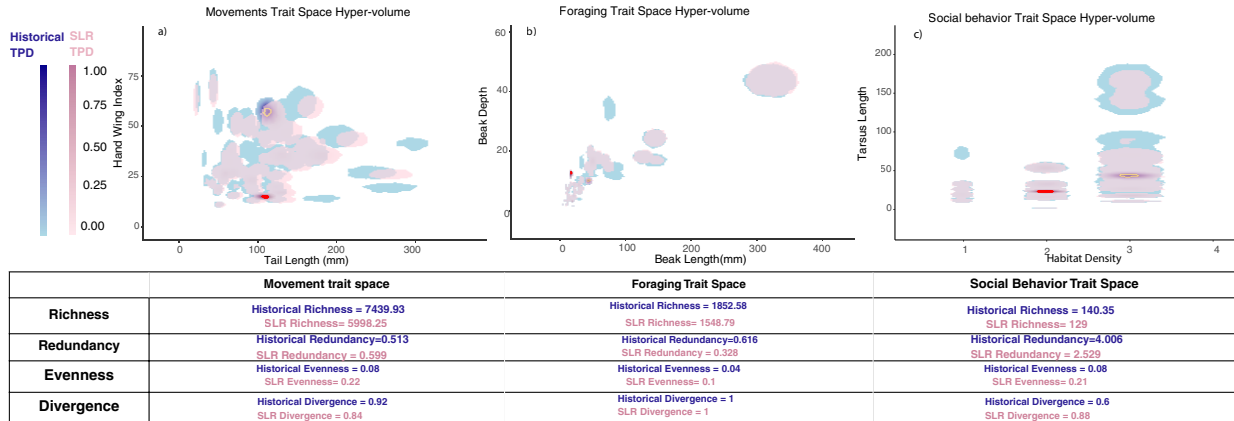


Figure 5. Functional trait probabilistic hypervolumes across the study area (probability density of the full range of species traits combinations of all present species) in three functional trait spaces with and without sea level rise impacts: movement, foraging, and social behavior trait spaces, and the table quantitative functional trait diversity index values. Function trait diversity index includes richness, redundancy, evenness, and divergence. Hand Wing Index and Tail Length combination composites movement space, Beak Depth and Beak Length composites foraging trait space, and Tarsus Length and Habitat Density composite social behavior space. The adjacent table lists all functional diversity indices for all three spaces in scenarios with and without sea level rise. Historical scenario without sea level rise is represented by blue color hypervolumes and index numbers, and sea level rise scenario is represented by pink color hypervolumes and index numbers. Highlight circles indicate the top 25% of the highest probability trait combinations within each space (yellow circle for historical scenario and red circle for SLR scenarios).

How well do protected areas protect biodiversity when sea levels rise

We looked into two National Estuarine Research Reserves (NERRs) -- Grand Bay, MS, and Weeks Bay, AL -- and used detailed simulations of marsh productivity change with SLR to see how well conservation areas can help preserve biodiversity under SLR (Figure 6). Treating the two coastal reserves as a single assemblage, the realized functional hypervolume (the probability density over the full range of species trait combinations of all present species in the bay areas) under SLR is maintained or expanded and becomes more evenly distributed across trait space. The clearest gains occur in movement traits: occupied volume increases, evenness rises, and redundancy climbs, indicating more strategies present, used more uniformly, and with greater “backup” among shore-connected movement modes. Foraging traits also show higher richness and evenness at the coast. However, redundancy remains very low (despite small increases), signaling that trophic resiliency is still limited even where trait breadth is high. Social traits exhibit moderate volume increases with conspicuous gains in evenness and redundancy, consistent with a broader, better-buffered mix of social strategies along protected shorelines. Across the two reserves, divergence either holds (movement) or nudges up (foraging/social), implying persistent availability of edge strategies for preserving biodiversity.

At the regional scale (coast + inland), the community’s hypervolume contracts under SLR: trait richness declines, evenness rises (more uniform use of a smaller space), and redundancy changes are group-specific—movement redundancy can increase even as foraging and social redundancy decline. The reserve aggregate sits at the opposite end of that gradient: along the coastal edge, trait volume is larger or preserved, use is more even, and redundancy is steady or higher (especially for movement and social traits) with SLR. In short, coastal reserves serve as trait refugia, while the inland/mid-elevation mosaic trends are primarily behind the regional contraction and biodiversity loss patterns shown.

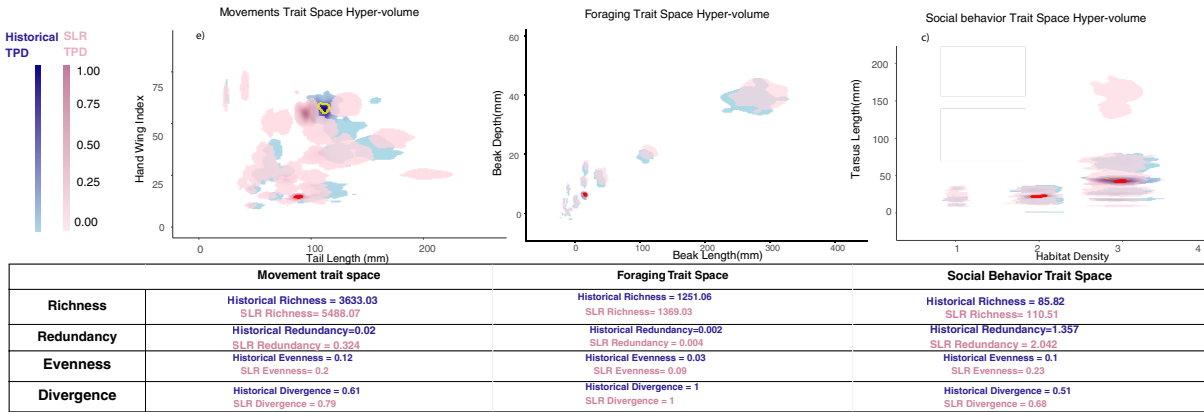


Figure 6. Functional trait probabilistic hypervolumes across two National Estuarine Research Reserves (NERRs) -- Grand Bay, MS, and Weeks Bay, AL, in three functional trait spaces, movement, foraging, and social behavior, with and without sea level rise impacts, and the table of quantitative functional trait diversity index values. Highlight circles indicate the top 25% of the highest probability trait combinations within each space (yellow circle for historical scenario and red circle for SLR scenarios).

Discussion

Anticipating that biodiversity changes in response to global environmental change (Olden et al., 2008) to inform conservation and restoration actions requires ecological forecasts that resolve patterns at both species and community levels. Conservation has traditionally focused on species counts (richness, abundance, endemism), but functional traits and their community-level patterns add another crucial dimension for planning and resilience.

Our AI hurdle model—coupling occurrence and abundance prediction in a two-stage manner while aligning both predictions to a shared latent space—captured fine-scale, nonlinear species–environment relationships while borrowing statistical strength across taxa via learned species embeddings. This structure enabled generative (zero-shot) expected-abundance predictions for sparsely observed species by positioning them in the label-embedding space informed by the rich ecological context of species harmonization and competition. The learned embeddings also yielded coherent interspecific association patterns and environmental change–species distribution response structure, providing an interpretable bridge between black-box predictions and ecological insight.

Spatially explicit functional diversity maps (richness, redundancy, evenness, divergence) revealed a consistent change gradient under sea-level rise (SLR). First, coastal cells (barrier-island rims, back-barrier marshes, estuarine margins) generally show increases or maintenance of functional richness with redundancy holding steady, while evenness rises, indicating more uniform participation among movement strategies without dominance by a few traits. Second, the largest richness losses concentrate in a coast-parallel, mid-elevation lower uplands just landward of the shoreline, where habitat conversion and edge losses exhibit the strongest decline of biodiversity. Third, upland areas exhibit strong increases in redundancy despite small declines in richness—an inland functional homogenization signal consistent with the consolidation of overlapping strategies as unique combinations and diversity are lost.

Trait-group-specific hypervolume analyses clarify how this reorganization occurs at the regional community level. The movement hypervolume shrinks regionally yet retains edge-weighted functional diversity and gains redundancy and evenness, implying fewer distinct movement trait combinations overall but more overlap and more uniform use among those that remain after SLR. The foraging hypervolume contracts as divergence increases and redundancy declines, suggesting pruning of intermediate strategies and a shift toward more extreme foraging modes with reduced resilience of functional traits. The social-behavior hypervolume narrows modestly, evenness rises, and divergence falls, indicating a center-ward shift with fewer extreme social strategies or traits.

When we studied the coastal reserves within the study area (Grand Bay NERR, MS; Weeks Bay NERR, AL), their joint hypervolumes expand or are maintained and fill more evenly across movement, foraging, and social traits; redundancy rises notably for movement and social domains, while foraging redundancy remains comparatively low. In contrast, at the whole-region scale (coast + inland), the overall hypervolume contracts, mid-elevation cells drive biodiversity loss, and uplands also experience trait homogenization. Together, these results position the reserves as functional diversity refugia—places where trait breadth and balanced use persist or improve under SLR—embedded in a surrounding landscape that is losing unique combinations and converging toward fewer traits.

Our analysis showed that no single biodiversity metric tells the whole story. Sea-level rise (SLR) often raises evenness—abundances become more uniformly distributed across the trait combinations that remain, which can be read as greater short-term resiliencies against further disturbance. But read in isolation, evenness can be misleading. Our trait diversity maps and hypervolumes show that these evenness gains frequently occur within a contracted trait space with lower biodiversity (functional diversity). In other words, communities may appear more “balanced” while simultaneously losing unique trait combinations that underpin rare or specialized functions, which can be understood as irreversible harm to ecosystems and biodiversity.

These spatially explicit findings can be translated into clear guidance for biodiversity conservation. 1) Trophic failure remains the weak link, as coastal foraging redundancy remains low despite gains in richness and evenness. 2) Strengthen prey and habitat diversity and cross-habitat linkages by restoring oyster-marsh-seagrass mosaics, securing fresh-brackish flow pulses (seasonal freshwater releases), plus local nutrient/turbidity management and seasonal protections for sensitive flats. 3) Preserve social-strategy complementarity by protecting both colonial and solitary sites and roost-forage corridors, supported by dynamic buffers and evidence-based predator management. 4) Convert coastal capacity into continuity by keeping tidal corridors open and edge habitats intact (living shorelines, marsh-platform maintenance, strategic sediment placement). 5) A dynamic buffer zone can be used around colonies to sustain functional traits and optimize management at reserve scales. 6) Finally, plan beyond reserve boundaries—use corridor easements and rolling setbacks to secure landward pathways and blunt inland homogenization.

Taken together, our results provide a tractable blueprint for biodiversity conservation actions. The approach used here to model the entire ecosystem of bird species demonstrates a novel way for ecologists and decision-makers to forecast and monitor biodiversity everywhere.

References and Notes

- Adams, N., Dias, T., Skeen, H. R., Pegan, T., Willard, D. E., Winger, B., Ruegg, K., Weeks, B. C., & Bay, R. (2025). Genetic and morphological shifts associated with climate change in a migratory bird. *BMC Biology*, 23(1), 3. <https://doi.org/10.1186/s12915-024-02107-5>
- Bayard, T. S., & Elphick, C. S. (2011). Planning for Sea-level Rise: Quantifying Patterns of Saltmarsh Sparrow (*Ammodramus Caudacutus*) Nest Flooding Under Current Sea-level Conditions. *The Auk*, 128(2), 393–403. <https://doi.org/10.1525/auk.2011.10178>
- Biggs, C. R., Yeager, L. A., Bolser, D. G., Bonsell, C., Dichiera, A. M., Hou, Z., Keyser, S. R., Khursigara, A. J., Lu, K., Muth, A. F., Negrete, B., & Erisman, B. E. (2020). Does functional redundancy affect ecological stability and resilience? A review and meta-analysis. *Ecosphere*, 11(7). <https://doi.org/10.1002/ecs2.3184>
- Cook, A., Cohen, J., & Kocek, A. (2024). Suboptimal conditions lead to differences in habitat use and nest survival of imperiled tidal marsh sparrows between an urban marsh and nearby non-urban island. *Avian Conservation and Ecology*, 19(2), art15. <https://doi.org/10.5751/ACE-02719-190215>
- Dias, M. P., Martin, R., Pearmain, E. J., Burfield, I. J., Small, C., Phillips, R. A., Yates, O., Lascelles, B., Borboroglu, P. G., & Croxall, J. P. (2019). Threats to seabirds: A global assessment. *Biological Conservation*, 237, 525–537. <https://doi.org/10.1016/j.biocon.2019.06.033>
- Elith, J., & Leathwick, J. R. (2009). Species distribution models: Ecological explanation and prediction across space and time. *Annual Review of Ecology, Evolution, and Systematics*, 40, 677–697. <https://doi.org/10.1146/annurev.ecolsys.110308.120159>
- Galbraith, H., Jones, R., Park, R., Clough, J., Herrod-Julius, S., Harrington, B., & Page, G. (2005). *Global Climate Change and Sea Level Rise: Potential Losses of Intertidal Habitat for Shorebirds*.
- Intergovernmental Panel on Climate Change (IPCC). (2023). Oceans and Coastal Ecosystems and Their Services. In *Climate Change 2022 – Impacts, Adaptation and Vulnerability* (pp. 379–550). Cambridge University Press. <https://doi.org/10.1017/9781009325844.005>
- MCGILL, B., ENQUIST, B., WEIHER, E., & WESTOBY, M. (2006). Rebuilding community ecology from functional traits. *Trends in Ecology & Evolution*, 21(4), 178–185. <https://doi.org/10.1016/j.tree.2006.02.002>
- NOAA. (2022). *2022 Sea Level Rise Technical Report: Infographics*.
- Pearson, R. G., & Dawson, T. P. (2003). Predicting the impacts of climate change on the distribution of species: Are bioclimate envelope models useful? *Global Ecology and Biogeography*, 12(5), 361–371. <https://doi.org/10.1046/j.1466-822X.2003.00042.x>
- Reynolds, M. H., Courtot, K. N., Berkowitz, P., Storlazzi, C. D., Moore, J., & Flint, E. (2015). Will the effects of sea-level rise create ecological traps for Pacific island seabirds? *PLoS ONE*, 10(9). <https://doi.org/10.1371/JOURNAL.PONE.0136773>

- Rosenberg, K. V., Dokter, A. M., Blancher, P. J., Sauer, J. R., Smith, A. C., Smith, P. A., Stanton, J. C., Panjabi, A., Helft, L., Parr, M., & Marra, P. P. (2019). Decline of the North American avifauna. *Science*, 366(6461), 120–124. <https://doi.org/10.1126/science.aaw1313>
- Saintilan, N., Wilson, N. C., Rogers, K., Rajkaran, A., & Krauss, K. W. (2014). Mangrove expansion and salt marsh decline at mangrove poleward limits. *Global Change Biology*, 20(1), 147–157. <https://doi.org/10.1111/gcb.12341>
- Seavey, J. R., Gilmer, B., & McGarigal, K. M. (2011). Effect of sea-level rise on piping plover (*Charadrius melanodus*) breeding habitat. *Biological Conservation*, 144(1), 393–401. <https://doi.org/10.1016/j.biocon.2010.09.017>
- Thuiller, W., Araújo, M. B., Pearson, R. G., Whittaker, R. J., Brotons, L., & Lavorel, S. (2004). Uncertainty in predictions of extinction risk. *Nature*, 430(6995), 34–34. <https://doi.org/10.1038/nature02716>
- Violle, C., Navas, M., Vile, D., Kazakou, E., Fortunel, C., Hummel, I., & Garnier, E. (2007). Let the concept of trait be functional! *Oikos*, 116(5), 882–892. <https://doi.org/10.1111/j.0030-1299.2007.15559.x>
- Violle, C., Thuiller, W., Mouquet, N., Munoz, F., Kraft, N. J. B., Cadotte, M. W., Livingstone, S. W., & Mouillot, D. (2017). Functional Rarity: The Ecology of Outliers. *Trends in Ecology & Evolution*, 32(5), 356–367. <https://doi.org/10.1016/j.tree.2017.02.002>
- Yan, Y., Shao, B., & Davis, C. C. (2024). A generative deep learning approach for global species distribution prediction. <https://doi.org/10.1101/2024.12.10.62784>

Acknowledgments: We thank Professor Ben Halpern (Director, NCEAS) for insightful comments and guidance during manuscript development, and Courtney Scarborough (Deputy Director, NCEAS) for helpful comments and assistance with manuscript editing. This paper is a result of research funded by the National Oceanic and Atmospheric Administration's RESTORE Science Program (ROR - <https://ror.org/0042xzm63>) under award NA22NOS4510203 to the National Center for Ecological Analysis and Synthesis (NCEAS) at the University of California, Santa Barbara, and part of the (Insert working group name) of the Gulf Ecosystem Initiative.

Funding:

National Oceanic and Atmospheric Administration: RESTORE Science Program grant NA22NOS4510203

Author contributions:

Conceptualization: LL, JB, MZ, HL

Methodology: LL, JB, SS, ZW, DF

Investigation: LL, SS, ZW

Visualization: LL

Project administration: HL

Supervision: DF

Writing – original draft: LL

Writing – review & editing: All coauthors

Competing interests: Authors declare that they have no competing interests.

Data and materials availability: All data, code, and materials used in the analysis will be made available on Dryad and Zenodo

Supplementary Materials

Materials and Methods

Supplementary Text

Figs. S1 to S8

5 Tabe. S1. Species abundance maps for additional bird species not listed in the Main Text-

continued

References

Materials and Methods

Study area and data

Analyses were conducted at 3km×3km spatial resolution on the northern Gulf of Mexico coast, including the southeastern parishes of Louisiana, the coastal counties of Mississippi and Alabama, and the western counties of the Florida panhandle. The study area aligned with the National Centers for Coastal Ocean Science project on Predicting Impacts of Sea Level Rise in the Northern Gulf of Mexico (NCOOS, 2017). All the required simulated data to create SLR scenarios are available for this study area, such as Bathymetry DEM (NOAA National Geophysical Data Center, 2010) and marsh productivity change with sea level rise for three National Estuarine Environmental Research Reserves: Apalachicola, FL, Weeks Bay, AL, and Grand Bay(Alizad et al., 2016). Our study drew on findings from studies examining the impact of SLR on coasts and coastal habitats, translating them into species response information to inform conservation and ecosystem management.

We used observation records from eBird (Sullivan et al., 2009) from 2019 to 2021, which included up to 115,575 checklist occurrences and counts after filtering, along with sampling-event metadata (e.g., protocol, duration, distance traveled, number of observers, start time). The filtering procedure followed the one described in (Li et al., 2025). Data was acquired and merged into one year for data augmentation. Checklists of all species were summarized into a table of species observations, with each shared locality ID represented as a single row in the table. The data version used in this study was the eBird Reference Dataset from 2025. To derive detections and non-detections, we restricted analyses to **Complete Checklists**—checklists where observers report all species they could identify during the sampling event—so that species not reported can be treated as absences on that checklist. Species responses were aggregated to the modeling grid with a 1km buffer. We modeled all **350 bird species** within the study area for two targets per 3km*3km grid cell: (i) **occurrence** (presence/absence) and (ii) **abundance/count** (non-negative), only excluding species with fewer than 10 observations over the three years through January, 2019 to December, 2021. Taxonomy and nomenclature follow the **eBird taxonomy 2020**.

Environmental covariates were assembled, tabulated, and standardized prior to modeling. Predictors included: **topography** (Amatulli et al., 2018)—mean elevation, elevation variability, slope, and aspect decomposed to **northness** and **eastness**; **Land cover**—proportional cover from C-CAP/land-cover classes aggregated to the grid (NOAA, 2024); climate-mean temperature and temperature range, and primary productivity of ecosystem- biomass concentration, and chlorophyll concentration. A full description of the list of data used and data sources can be found in this Supplementary Information. A climate change and sea level rise scenario is created by modifying the historical prediction surface with replaced temperature under climate change from Bio-ORACLE (Assis et al., 2024) and WorldClim2 (Fick & Jijmans, 2017) for ocean and land,

respectively, and land cover classes with marsh migration (Marcy et al., 2011) (accessed at <https://coast.noaa.gov/slodata/>). The projected temperature was acquired for CMIP6 SSP5-8.5, matching the intermediate high sea level rise scenario (1.2 m above the mean sea surface level by 2100) (Parris et al., 2012). We utilized Mean High Water and Salt Marsh Productivity data from the NOAA National Centers for Environmental Information (Alizad et al., 2018), which were modeled using Hydro-MEM (Alizad et al., 2016), to modify the historical bathymetry, digital elevation, and primary productive predictors (biomass concentration and chlorophyll concentration) for the three National Estuarine Research Reserves.

To enable trait-based comparisons, species were cross-walked to a curated trait table via eBird taxonomy and the AVONET bird species trait table (Tobias et al., 2022a). Categorical traits, including **Habitat**, **Primary Lifestyle**, **Trophic Level**, **Trophic Niche**, and **Migration status**, were used to categorize trait probability density, trait analysis, and draw separate graphs. Continuous traits, such as **Tarsus Length**, **Habitat Density**, **Tail length**, and **wing length**, were used for trait probability density (TPD) surface estimation, with non-zero support delineated for interpretability.

Generative Variational Autoencoder with Gaussian Mixture

Utilizing citizen science data for species occurrence and count observations requires a robust model structure to account for data noise across time and space (Elith et al., 2006). AI SDMs have been proven to outperform traditional machine learning models to handle such noise (Lee et al., 2022). We follow a generative framework of Gaussian Mixture Variational Autoencoders (Bai et al., 2021a), which allows for zero-shot learning (predicting for species not seen during training) (Yan et al., 2024). The architecture consists of two parallel encoders, feature and label encoders, a shared latent representation, and two decoders, each designed to align and reconstruct feature and label modalities (Fig. S1).

Environmental feature vectors X at a location/time (e.g., land-cover fractions, elevation stats, temperature means/ranges, chlorophyll, etc.) were first standardized and then passed through a multi-layer perceptron (MLP) (Rumelhart et al., 1986) (three fully connected layers of 256, 512, 256 neurons respectively) with rectified linear unit (ReLU) activations and dropout regularization. Outputs μ_x (mean), $\log \sigma_x^2$ (log variance) are mapped to a latent Gaussian distribution ($\epsilon \sim \mathcal{N}(0, I)$) and reparametrized by μ_x and $\log \sigma_x^2$, generating a reparametrized latent sample z_x for the feature label path. Species occurrence or abundance labels j were embedded and projected through a symmetric encoder consisting of fully connected layers (embedding dimension $\rightarrow 512 \rightarrow 256$ neurons) with ReLU activations and dropout. The resulting output (mean μ_s , variance $\log \sigma_s^2$ per species) was parameterized into a Gaussian distribution. Reparameterization step (Equation 1) that ensured differentiability while capturing uncertainty in the latent variables:

$$z = \mu + \epsilon \odot \sigma, \quad \epsilon \sim \mathcal{N}(0, I). \quad \text{Equation 1}$$

And each label was further modeled as a component of a Gaussian mixture, enabling mixture-based latent modeling. The **Gaussian Mixture Variational Autoencoder (GMVAE)** prior (Bai et al., 2021) in the latent space allows each species label to be associated with a distinct mixture component, supporting **zero-shot prediction** (Yan et al., 2024).

Both encoders produced distributions from which latent codes were sampled using the reparameterization trick (Equation 1). Latent variables were passed through two decoding pathways: The Feature Decoder h_y concatenated latent codes with input features and projected them through two fully connected layers to generate normalized embeddings in the shared space. The Label Decoder h_x concatenated latent codes with feature embeddings and projected them through fully connected layers with leaky ReLU activation to generate label embeddings. A reconstruction branch directly attempted to reconstruct the original features from the latent codes, ensuring information preservation. Both feature and label decoders were aligned into a shared embedding space. A learned linear transformation then mapped embeddings back into the label space ($W_{emb} \cdot h \rightarrow \eta$), enabling final predictions of species occurrence probability or abundance.

Model training was conducted using Pytorch Lightning (Falcon, 2019) with GPU acceleration where available. The **Adam optimizer** was applied with separate initial learning rates of $5e^{-3}$ and $2e^{-4}$ for classification and regression, respectively. These rates decayed by a factor of 0.5 if the validation loss did not improve for four epochs, using a **StepLR** scheduler. All experiments were repeated across 70%/15%/15% train/validation/test partitions using a fixed random seed (42) to ensure robustness, and results were reported as the mean \pm standard deviation of evaluation

metrics. TorchMetrics was used for accuracy, RMSE evaluation. Models were trained for a maximum of 500 epochs each for classification and regression. The regressor VAE was trained while the classifier was frozen/evaluation. During this phase, the regressor consumed the classifier's sigmoid presence probabilities (computed without gradient) to gate abundance predictions. No gradient clipping and no early stopping were applied. The mini-batch size was 4096 for all experiments.

Each VAE uses the same internal components as described above (feature encoder/decoder and label encoder/decoder) but is trained with task-specific likelihoods inside a composite objective. Let L_{NLL} denote the prediction negative log-likelihood terms (both the label-decoder path and two feature-decoder-based paths), L_{KL} the latent KL divergence (GMVAE regularization) (Kingma & Welling, 2022), and L_{CPC} the contrastive alignment loss (Bai et al., 2021b; Khosla et al., 2021). Loss contributions were weighted such that NLL received primary emphasis ($\alpha=10$), KL divergence was scaled by $\beta=6$ to balance reconstruction and regularization, and CPC alignment was scaled by $\gamma=1$ (Kong et al., 2020). During training, the weighted sum of loss (Equation 2) was minimized:

$$\mathcal{L}_{total} = \alpha \cdot (\mathcal{L}_{NLL,Label} + \mathcal{L}_{NLL,feat} + \mathcal{L}_{NLL,feat2}) + \beta \cdot \mathcal{L}_{kl} + \gamma \cdot \mathcal{L}_{CPC} \quad \text{Equation 2}$$

Two-stage hurdle structure

A two-stage hurdle approach (Kong et al., 2020) was used to model species abundance distribution for 350 species informed by occurrence modeling results. A hurdle model is a two-part model that specifies two separate processes, one for generating zero values and another for generating values given that they are non-zero, for handling count observations with excess zeros (Edmondson et al., 2021).

In this study, the first stage is using the Multivariate Probit Model (Chen et al., 2016) to model the presence/absence of each species, capturing interspecies and environment-species covariance. (Bai et al., 2020). This stage is treated as a *foundation model* (Dinnage, 2024) that provides ecological context. Building on the occurrence distribution, a second fine-tuned regression abundance model was trained using species count data with rich context informed by the occurrence model. For classification, the label decoder projects into a probability space through a sigmoid output layer, yielding predicted occurrence probabilities for each species (Presence head: $\eta_{bin} \rightarrow p = \text{sigmoid}(\eta^{bin})$). For regression, the decoder projects into a continuous output layer with linear activation, providing predicted species abundances.

Because both tasks share the same latent embedding, gradients from classification and regression jointly shape the latent space (Count head: $\eta_{cnt} \rightarrow \text{rate } \lambda = \exp(\eta_{cnt})$). This encourages the model to learn representations that are predictive of both species presence/absence and relative abundance, rather than optimizing them in isolation; therefore, it was named as cross-task regulation. This integration allows the model to flexibly shift between predicting occurrence and abundance depending on available data, while maintaining a unified ecological embedding space.

The NLL loss uses a hurdle formulation with two probabilistic heads: a Bernoulli component for presence and a Poisson component for conditional counts (Bishop, 2016; Huffer et al., 2008). During the **occurrence (classification) phase**, the classifier outputs a logit $\eta_{is}^{(bin)}$, converted to a probability $p_{is}=\sigma(\eta_{is}^{(bin)})$ with the logistic sigmoid $\sigma(\cdot)$. The Bernoulli negative log-likelihood (equivalently, binary cross-entropy), averaged over samples and species, is

$$\mathcal{L}_{bern} = -\frac{1}{NS} \sum_{i=1}^N \sum_{s=1}^S [y_{is}^{bin} \log p_{is} + (1 + y_{is}^{bin}) \log (1 - p_{is})]$$

Let x_i denote environmental features for sample $i=1,\dots,N$ and $y_{is}^{bin} \in \{0,1\}$ the presence/absence of species $s=1,\dots,S$. When present, the observed count is $y_{is}^{cnt} \in N$.

During the **Abundance (regression) phase**, the standard Poisson log-likelihood with **log link** (Cameron & Trivedi, 2013; Kingma & Welling, 2022) was used, which was restricted to the positive (post-hurdle). The regressor outputs an unconstrained value $\eta_{is}^{(cnt)}$ that parameterizes the Poisson rate $\lambda_{is}=\exp(\eta_{is}^{(cnt)})$. A small L_{aux} auxiliary term to stabilize rate

estimates. Counts are modeled only when a species is present via the hurdle mask $m_{is} = y_{is}^{\text{bin}}$. The presence indication **masked the Poisson** loss to respect the hurdle structure.

$$\mathcal{L}_{pois} = \frac{1}{\sum_{i,s} m_{is}} \sum_{i=1}^N \sum_{s=1}^S m_{is} (\lambda_{is} - y_{is}^{\text{cnt}} \log \lambda_{is})$$

$$\mathcal{L}_{aux} = \delta \frac{1}{\sum_{i,s} m_{is}} \sum_{i,s} m_{is} (\lambda_{is} - y_{is}^{\text{cnt}})$$

5 For training, validation, and test, raw sigmoid outputs from the classifier's feature path were binarized using data-adaptive, species-specific thresholds: for species with batch mean probability > 0.01 , we used the batch column mean as the threshold (probability $>$ mean $\rightarrow 1$), and for lower-prevalence species we used a fixed threshold of 0.05 (probability $> 0.05 \rightarrow 1$).

10 During **regressor training**, the classifier's **probabilities** are used to **gate** abundance predictions: if the presence probability < 0.01 , the predicted abundance is set to 0. Bias is more prominent in count observations. Observers may record thousands of birds without counting them; therefore, the larger the count is, the bigger the error may be. To mitigate observer-related biases, we train the abundance model using log-transformed counts rather than raw counts. Predictions are then back-transformed to the original scale and rounded to integers for evaluation with **mean**
15 **squared error (MSE)**. The alignment between where species are present and the predicted number of individuals is assured by the Contrastive Learning (Bai et al., 2021c). Occurrence and abundance predictions are linked through the shared latent space: the presence model constrains abundance estimates, encouraging the hybrid model to learn biologically realistic joint representations of occurrence and abundance.

20 Classification and regression were evaluated using different sets of metrics. Classification used Accuracy, F1-score, Precision, Recall, and Intersection over Union (IoU). These metrics captured different aspects of predictive performance, with IoU providing a robust measure of overlap between predicted and observed species presence. Additionally, reliability diagrams and Brier scores were used to assess the degree to which predicted probability models matched observed frequencies. Regression used Root Mean Squared Error (RMSE) and Mean Absolute Error
25 (MAE). RMSE emphasized large deviations between predicted and observed abundance values, while MAE provided a more interpretable measure of average prediction error. Together, these metrics provided a comprehensive evaluation of predictive accuracy, robustness, and ecological interpretability across the two modeling tasks.

30 For downstream analyses, we saved monthly prediction surfaces and summary arrays for evaluation metrics (e.g., F1, precision/recall, calibration, richness, and community dissimilarity indices). The trained model also yields a **512-dimensional feature embedding per species** (array shape **350×512**) and a **350×350** residual correlation embedding used to interrogate interspecific co-occurrence patterns beyond environmental effects.

Species environmental and biotic envelope analysis

35 To present the species' environmental envelope learned by the hurdle model, we assembled a paired dataset combining environmental grids used for predictions and the predicted abundance expectation from the deep hurdle model. A monotonic association using **Spearman's rank correlation** was calculated for each species abundance expectation and feature at the same prediction grid. Spearman ρ is robust to nonlinearity and scale differences common in ecological predictors and count-like responses. Operationally, each column of Y was rank-transformed for each aligned environmental predictor row, standardized (with a mean of zero and a variance of one), and then computed as
40 a Pearson correlation on the ranks. Collecting all pairs yields a **species × feature association matrix** \mathcal{R}_{sf} . An agglomerative hierarchical clustering (average linkage) was applied to the dissimilarity ($1 - \mathcal{R}$), with γ clipping to $[-1, 1]$ for stability. And rows and columns were reordered according to the order of the dendrogram's leaves.

We summarized species–species associations in the model’s label embedding space by computing a pairwise correlation matrix among species’ embedding vectors. We first mean-centered each vector across embedding dimensions. Then we calculated Pearson correlations, yielding a species-by-species symmetric matrix \mathcal{R}_{ss} with a unit diagonal (Set the diagonal to 0 for visualization only). Again, an agglomerative hierarchical clustering (average linkage) was applied to the dissimilarity ($1 - R$), with γ clipping to the range of $[-1, 1]$ for numerical stability (Figure 2B).

For visualization, we set the diagonal to zero (display only). Hence, the color scale emphasizes interspecific associations, and we scaled the colormap limits to the 2nd–98th percentiles of off-diagonal values to enhance contrast while remaining robust to outliers.

The resulting ordered correlation heat map provides a compact view of species that share similar or dissimilar embedding profiles—i.e., species predicted to exhibit positive residual association indicate similar abiotic niche (warm colors) or contrast indicate dissimilar abiotic niche (cool colors), based on the learned label embedding space from observations.

Because these are species correlations, strong positive links are best interpreted as **community clustering** around similar environments, while strong negative links point to species replacement rather than co-occurrence.

Trait Density Probability Analysis

Species traits were sourced from AVONET (Tobias et al., 2022b), a global compilation of avian morphology and ecology with species-level summaries derived from >90,000 measured individuals across 11,000+ species. However, only species-level mean traits were provided in AVONET. Intraspecific trait variation arising from genetic differences and phenotypic plasticity can be large enough to alter interaction outcomes and community assembly. Therefore, consideration of stochasticity in intraspecific trait differences is necessary to mitigate the risks of biasing trait distribution change predictions due to environmental changes.

We used continuous trait summaries in AVONET as standardized means for species-level continuous traits and categorical traits as categorical assignments. Continuous traits were converted to pseudo-individual values by parametric jittering with independent Gaussian draws using the species-level means from AVONET. A conservative coefficient of variation (5%) was imposed to reflect unobserved within-species variability in the absence of trait-specific variance estimates from AVONET. To align traits with our observation table, we expanded each species’ trait record to the number of observations for that species (n_s). When the trait was missing or zero, values were left as NA. Categorical traits (e.g., trophic niche, habitat, migratory status) were replicated deterministically across the n_s rows. This strategy preserves species identity while yielding an observation-aligned trait matrix in which continuous traits incorporate modest within-species dispersion to accommodate intraspecific variation that affects community assembly (Bolnick et al., 2011) when only species means are available.

We quantified species’ functional structure using the Trait Probability Density (TPD) approach implemented in the R package TPD (Adams et al., 2025; Carmona et al., 2019). The TPD framework represents each ecological unit (species, community) by a probability density function in trait space, enabling overlap-based measures of richness, dissimilarity, redundancy, and divergence.

Continuous traits (and, where mixed traits were present, ordination scores from) were scaled to zero mean and unit variance before analysis. Species-level probability densities were estimated using multivariate kernel density estimation, and returns species/population TPDs were evaluated on a regular grid. We set the probability isopleth at alpha = 0.95 to define the high-probability support (non-zero region) and controlled grid resolution via two divisions. We didn’t use a Gower–PCoA reduction to analyze the mixed traits space of continuous traits and categorical traits. Instead, we categorize species by their categorical traits and built three pair-wise 2-dimensional trait spaces, namely Beak Length/Beak Depth (indicating foraging trait space), Tail length/Hand Wing Index (indicating movement trait space), and Tarsus Length/Habitat Density (Indicating social behavior space). Tarsus length represents species size, and we regard species of different sizes as having distinct social behavior, as many studies have suggested (Adams et al., 2025; Delestrade, 2001; Weeks et al., 2020).

From species to communities, community-level densities were obtained for each of the three spaces, which mixes species probability density, weighted by their relative abundances in each sampling unit (here we used historical and sea level scenarios). This produces the Trait Probability Density (TPD) for each scenario, which is directly comparable for evaluating species resilience in response to sea level rise. We summarized and reported the functional structure using richness, evenness, redundancy, and divergence, all of which were computed on the probabilistic trait space. All analyses were conducted in the R programming language (R core team, 2021)

Supplementary Text

Data sources

- eBird data

The eBird data used to conduct this study are freely available on the eBird website at <https://ebird.org/science/use-ebird-data>. The data version used in this study was the eBird Reference Dataset from 2025

- Air Temperature (Mean and Range)

Ocean air temperature was acquired at <https://www.bio-oracle.org/downloads-to-email.php>
v.3.0 Assis, J., Fernández Bejarano, S.J., Salazar, V.W., Schepers, L., Gouvea, L., Frakopoulou, E., Leclercq, F., Vanhoorne, B., Tyberghein, L., Serrão, E.A., Verbruggen, H., De Clerck, O. (2024) Bio-ORACLE v3.0. Pushing marine data layers to the CMIP6 Earth system models of climate change research. *Global Ecology and Biogeography*. DOI: 10.1111/geb.13813
v.1.0 Tyberghein L, Verbruggen H, Pauly K, Troupin C, Mineur F, De Clerck O (2012) Bio-ORACLE: A global environmental dataset for marine species distribution modelling. *Global Ecology and Biogeography*, 21, 272–281. DOI: 10.1111/j.1466-8238.2011.00656.x

Land air temperature was acquired at <https://www.worldclim.org/data/index.html>
Citation: Fick, S.E. and R.J. Hijmans, 2017. WorldClim 2: new 1km spatial resolution climate surfaces for global land areas. [International Journal of Climatology 37 \(12\): 4302-4315](https://doi.org/10.1080/0267814X.2017.1302315).

- Topography

We retrieved information on elevation and topography (eastness and northness) from the following source(s):

Amatulli, G., S. Domisch, M.-N. Tuanmu, B. Parmentier, A. Ranipeta, J. Malczyk, and W. Jetz. 2018. Data descriptor: A suite of global, cross-scale topographic variables for environmental and biodiversity modeling. *Scientific Data* 5:180040. <https://doi.org/10.1038/sdata.2018.40>

[Data from Amatulli et al. \(2018\) available at](#)

https://www.avl.class.noaa.gov/saa/products/search?sub_id=0&datatype_family=VIIRS_SDR&submit.x=21&submit.y=5

- Chlorophyll Concentration

The terrestrial leaf chlorophyll content for the year of 2020 was acquired from Qian, X., Liu, L., Chen, X., Zhang, X., Chen, S., & Sun, Q. (2023). Global Leaf Chlorophyll Content Dataset (GLCC) from 2003–2012 to 2018–2020 Derived from MERIS and OLCI Satellite Data: Algorithm and Validation. *Remote Sensing*, 15(3), 700. <https://doi.org/10.3390/rs15030700>

Accessed 12/04/2024 at https://plus.figshare.com/articles/dataset/GLCC_global_leaf_chlorophyll_content_dataset_over_2003_2012_and_2018_2020_derived_from_MERIS_OLCI_satellite_data/20439351

The ocean chlorophyll concentration was acquired from SUOMI-NPP VIIRS Level-3 Mapped Chlorophyll, Version 2022

NASA Goddard Space Flight Center, Ocean Ecology Laboratory, Ocean Biology Processing Group. Visible and Infrared Imager/Radiometer Suite (VIIRS) SUOMI-NPP VIIRS Level-3 Mapped Chlorophyll; NASA OB.DAAC, Greenbelt, MD, USA. doi: 10.5067/SUOMI-

NPP/VIIRS/L3M/CHL/2022.

Accessed on 12/2/2024 at <https://oceancolor.gsfc.nasa.gov/l3/>

- Land / Ocean Biomass Density Merge (9 km)

5 GEDI L4B Gridded Aboveground Biomass Density, Version 2.1 (land)

Dubayah, R.O., J. Armston, S.P. Healey, Z. Yang, P.L. Patterson, S. Saarela, G. Stahl, L. Duncanson, J.R. Kellner, J. Bruening, and A. Pascual. 2023. GEDI L4B Gridded Aboveground Biomass Density, Version 2.1. ORNL DAAC, Oak Ridge, Tennessee, USA. <https://doi.org/10.3334/ORNLDAA/2299>

Accessed at https://daac.ornl.gov/cgi-bin/dsviewer.pl?ds_id=2299

10 We used SUOMI-NPP VIIRS Level-3 Mapped Particulate Organic Carbon, Version 2022 for the Ocean biomass density approximation

NASA Goddard Space Flight Center, Ocean Ecology Laboratory, Ocean Biology Processing Group. Visible and Infrared Imager/Radiometer Suite (VIIRS) SUOMI-NPP VIIRS Level-3 Mapped Particulate Organic Carbon Data; NASA OB.DAAC, Greenbelt, MD, USA. doi: 10.5067/SUOMI-

15 NPP/VIIRS/L3M/POC/2022.

Accessed on 12/2/2024 at <https://oceancolor.gsfc.nasa.gov/l3/>

Mapped Particulate Organic Carbon (units of mg C / m³) was super imposed on the GEDI L4B Gridded Aboveground Biomass Density

- CCAP Land use and land cover information

National Oceanic and Atmospheric Administration, Office for Coastal Management. "Name of Data Set." Coastal Change Analysis Program (C-CAP) Regional Land Cover. Charleston, SC: NOAA Office for Coastal Management. <https://coast.noaa.gov/digitalcoast/data/ccapregional.html>

25 Data were downloaded from https://coastalimager.blob.core.windows.net/ccap-landcover/CCAP_bulk_download/Regional_30meter_Land_Cover/index.html

- Bathymetry Digital Elevation Models

NOAA National Geophysical Data Center. 2010: Northern Gulf 1 arc-second MHW Coast Digital Elevation Model. NOAA National Centers for Environmental Information. Accessed 30 September 2024 at <https://www.ngdc.noaa.gov/iso?id=gov.noaa.ngdc.mgg.dem:731>

- Species trait database AVONET

Bird species traits were acquired from AVONET accessed at <https://figshare.com/s/b990722d72a26b5bfead>

35 Tobias, J. A., Sheard, C., Pigot, A. L., Devenish, A. J. M., Yang, J., Sayol, F., Neate-Clegg, M. H. C., Alioravainen, N., Weeks, T. L., Barber, R. A., Walkden, P. A., MacGregor, H. E. A., Jones, S. E. I., Vincent, C., Phillips, A. G., Marples, N. M., Montaño-Centellas, F. A., Leandro-Silva, V., Claramunt, S., ... Schleuning, M. (2022). AVONET: morphological, ecological and geographical data for all birds. *Ecology Letters*, 25(3), 581–597.

<https://doi.org/10.1111/ele.13898>

- Marsh Migration with Sea Level Rise

Land covers representing marsh migration with sea level rise were acquired from NOAA sea level rise viewer Data Download accessed at https://coastalimager.blob.core.windows.net/ccap-landcover/CCAP_bulk_download/Sea_Level_Rise_Wetland_Impacts/index.html

45 Marcy, D., Herold, N., Waters, K., Brooks, W., Hadley, B., Pendleton, M., & Schmid, K. (2011). *New Mapping Tool and Techniques For Visualizing Sea Level Rise And Coastal Flooding Impacts*, National Oceanic and Atmospheric Administration (NOAA) Coastal Services Center. www.csc.noaa.gov

- Mean High Water and Marsh Productivity with Sea Level Rise

50 The mean high water and marsh productivity changes with sea level rise for three National Estuarine Environmental Research Reserves were acquired from NCCOS Ecological Effects of

Sea Level Rise in the Northern Gulf of Mexico (EESLR-NGOM)

<https://www.ncei.noaa.gov/access/metadata/landing-page/bin/iso?id=gov.noaa.nodc:0170338>

Alizad, K., Hagen, S. C., Medeiros, S. C., Morris, J. T., Weishampel, J. F., Bilskie, M. v., Kidwell, D., Buckel, C., & Passeri, D. (2018). NCCOS Ecological Effects of Sea Level Rise in the Northern Gulf of Mexico (EESLR-NGOM): Mean High Water and Salt Marsh Productivity (Hydro-MEM) (NCEI Accession 0170338) - NCCOS - National Centers for Coastal Ocean Science. <https://doi.org/https://doi.org/10.7289/v5dr2srj>

Classification task evaluation by habitat preference trait

We presented the distribution of the evaluation matrix in the main text. Here, the confusion matrices of AI classification tasks were presented for each categorical habitat preference trait in Fig. S2. The share of true negatives (top row) and true positives (bottom row) that were predicted as 0 or 1. The bottom-right cell represents recall, and the top-right cell is the false-positive rate (FPR). Reported F1, precision (P), and recall (R) summarize each habitat's binary classifier.

The hurdle model is recall-oriented across habitats ($R \approx 0.67\text{--}0.84$), but precision is low ($P \approx 0.07\text{--}0.30$), as indicated by the confusion matrices, resulting in a moderate F1 score. This means it usually finds habitat-preferred cases but also raises many false alarms, especially when positives are rare. The general high zero rates across species observations posed challenges to species classification tasks. Best-classified results were produced for Marine birds ($F1 = 0.44$, $P = 0.30$, $R = 0.84$; $FPR = 13.8\%$) and Woodland birds ($F1 = 0.43$, $P = 0.30$, $R = 0.73$; $FPR = 15.7\%$). Many true marine cases are found, though ~14% of non-marine cases are flagged (precision 0.30). For Woodland species, the balanced classification with recall (R 0.73) is strong. The classification for Grassland birds ($F1 = 0.12$, $P = 0.07$, $R = 0.67$; $FPR = 8.6\%$)—recall is decent, but extremely low precision implies very low prevalence and overlap with other habitat birds models. Positive observations are so rare that precision collapses—typical when prevalence is very low.

Urban (Human-modified) bird models exhibit moderate classification performance ($F1 = 0.37$, $P = 0.25$, $R = 0.71$); anthropogenic structures enhance observation quality. Coastal birds prediction results have very high recall (0.80) but low precision (0.15), $F1 = 0.25$; shoreline cues are broad, so many non-coastal cells get flagged. Riverine is a linear habitat, leading to good sensitivity but many false positives ($F1 = 0.26$, $P = 0.16$, $R = 0.75$). For forest birds, $F1 = 0.22$ ($P = 0.13$, $R = 0.72$). Interior forests are detected, but edges/shared features inflate FPR (13.3%).

For future modeling efforts, consider prevalence-aware calibration, additional features (e.g., distance-to-shore, hydroperiod), or hierarchical labeling (e.g., marine/coastal → wetland/riverine → upland subclasses), which can potentially increase precision, especially for the habitat trait of grassland, coastal, wetland.

10

15

20

25

30

35

40

45

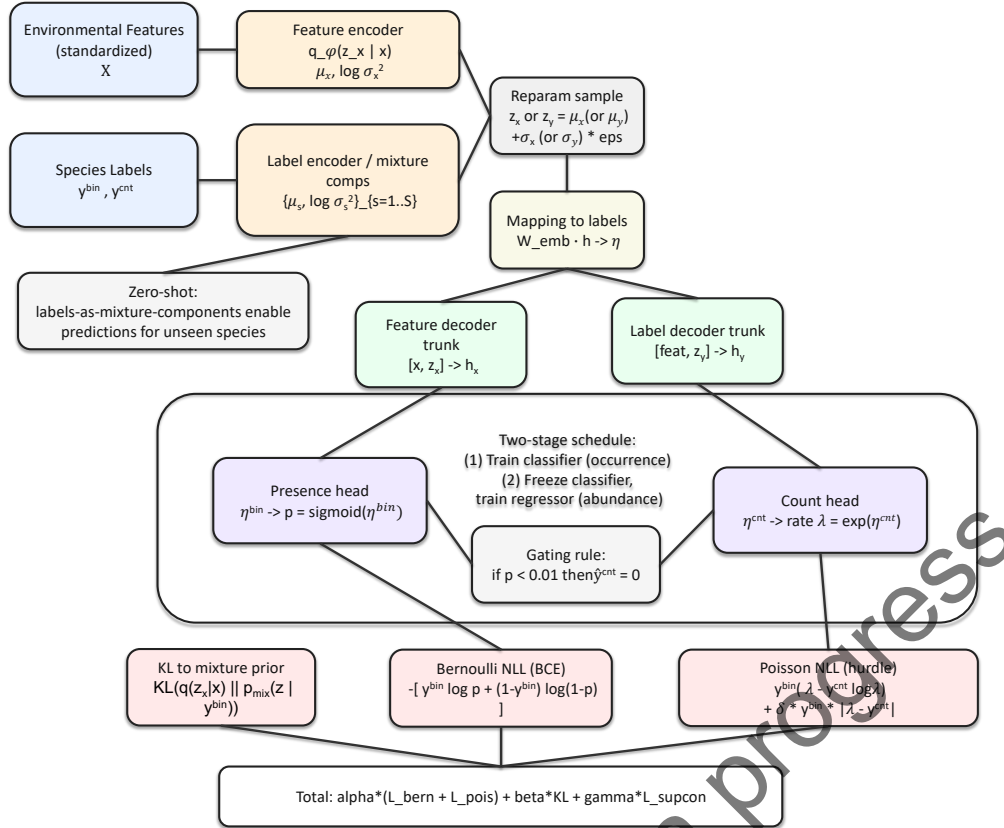


Fig. S1. Diagram of the Generative Variational Autoencoder with Gaussian Mixture in a hurdle framework (gate rule, conditional Poisson loss, and two-stage training schedules) for species abundance predictions gated by occurrence predictions

5

10

15

20

25

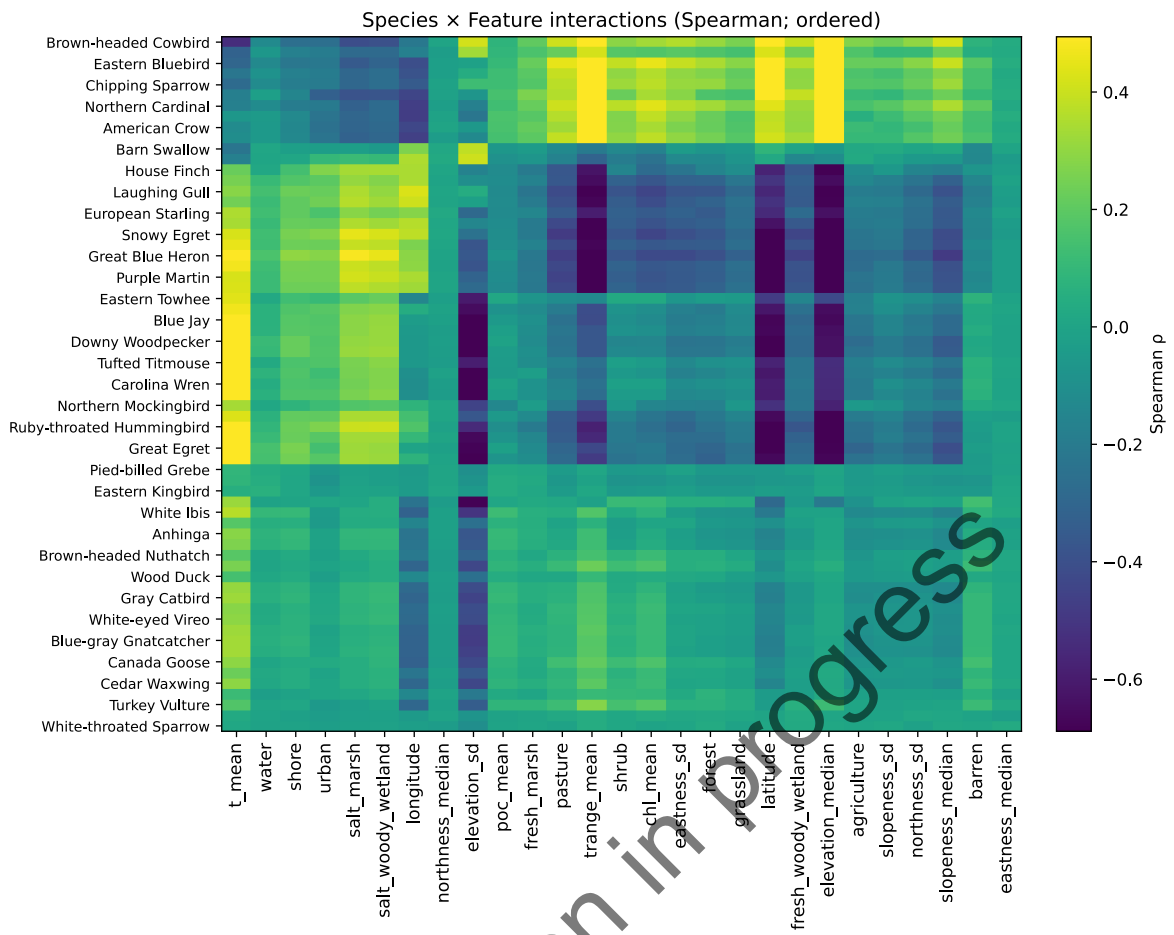
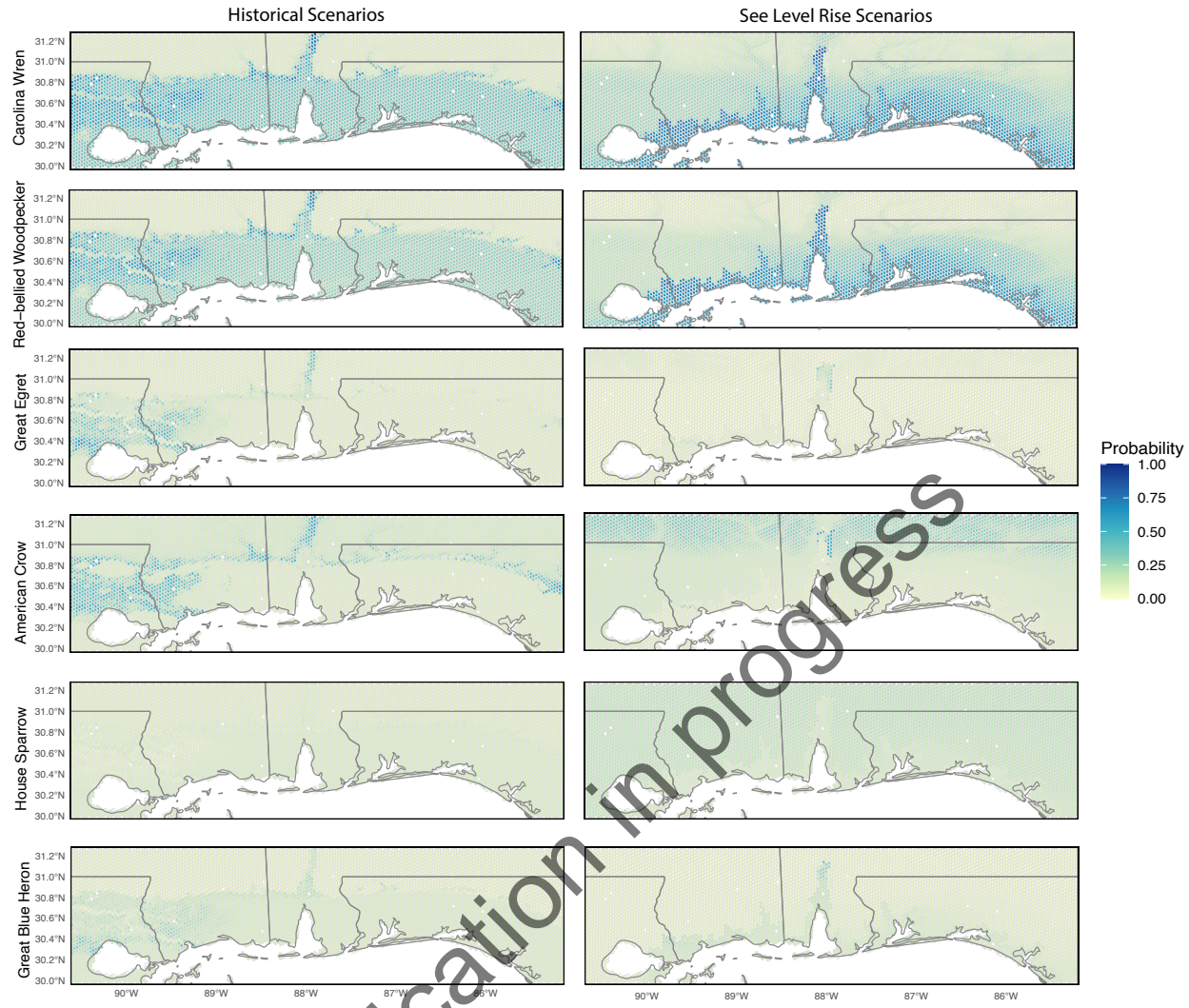


Fig. S2. Species-environment correlation (Spearman correlation) matrices

**Fig. S3.**

Maps of bird species occurrence probability from historical scenarios to sea level rise scenarios

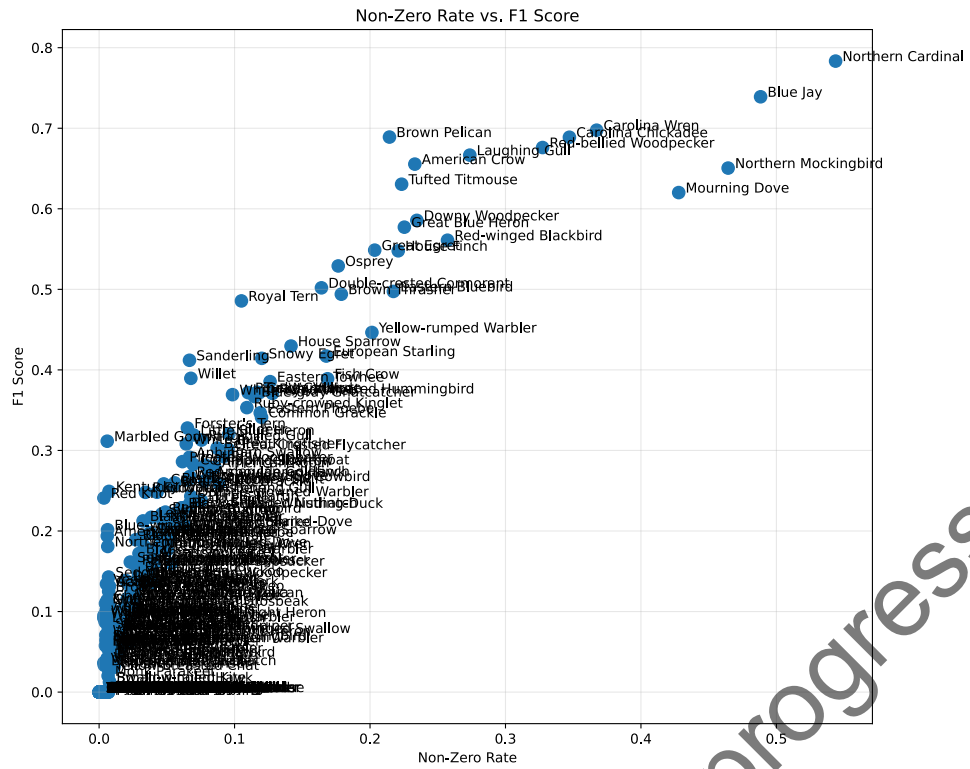


Fig. S4.

Classification performance represented by the F1 score vs. the Non-Zero Rate of species-level observations

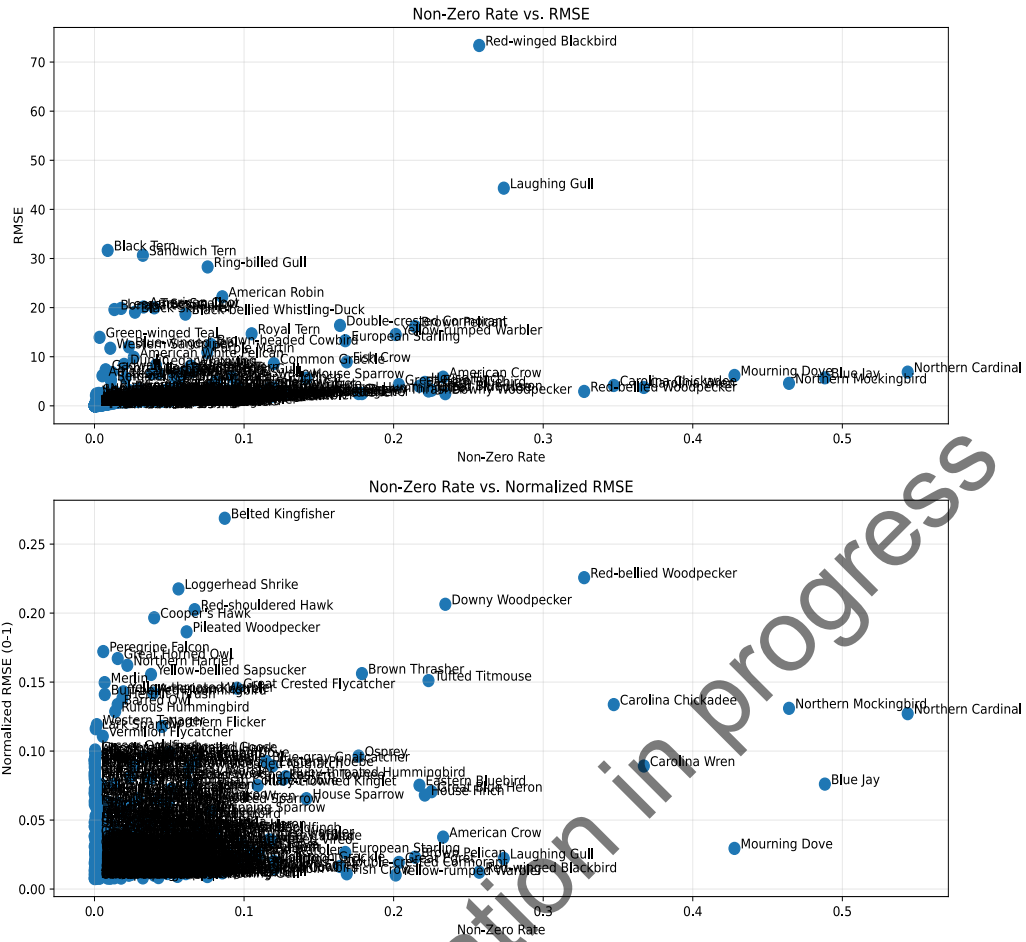
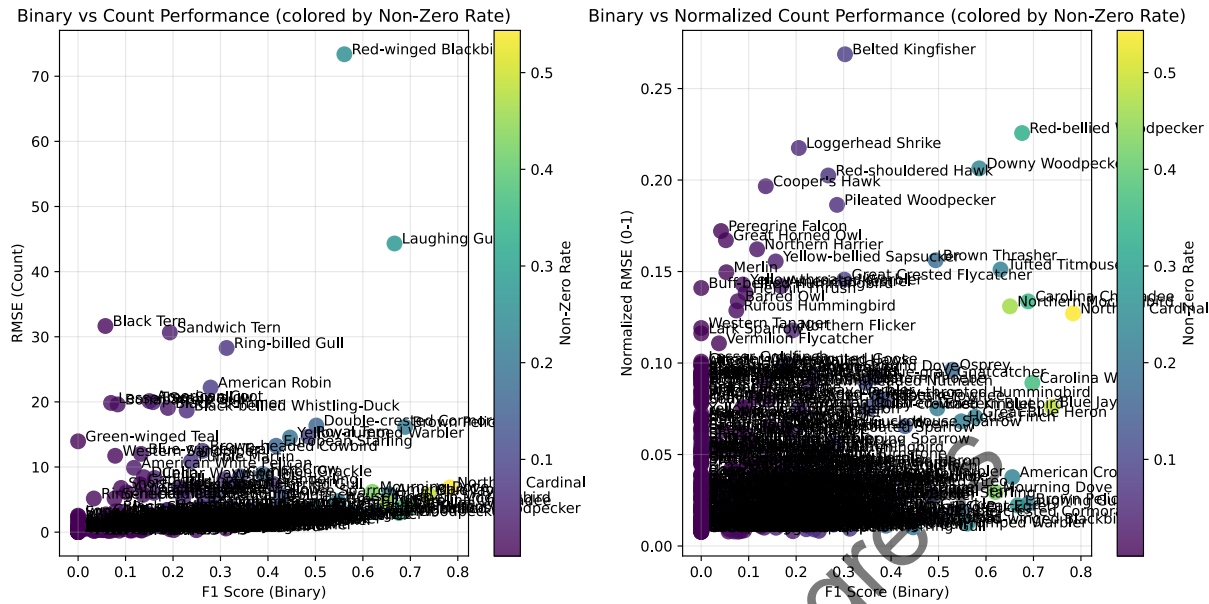


Fig. S5.

Regression performance indicated by the RMSE and Normalized RMSE (0-1) vs. the Non-Zero Rate of species-level observations

15

**Fig. S6.**

Binary classification performance (F1 score) vs. regression performance (RMSE and Normalized RMSE (0-1)).

5

10

15

20

25

30



Fig. S7. Confusion matrices for occurrence prediction (classification task) categorized using habitat preference trait (P: precision, R: Recall, N: number of instances)

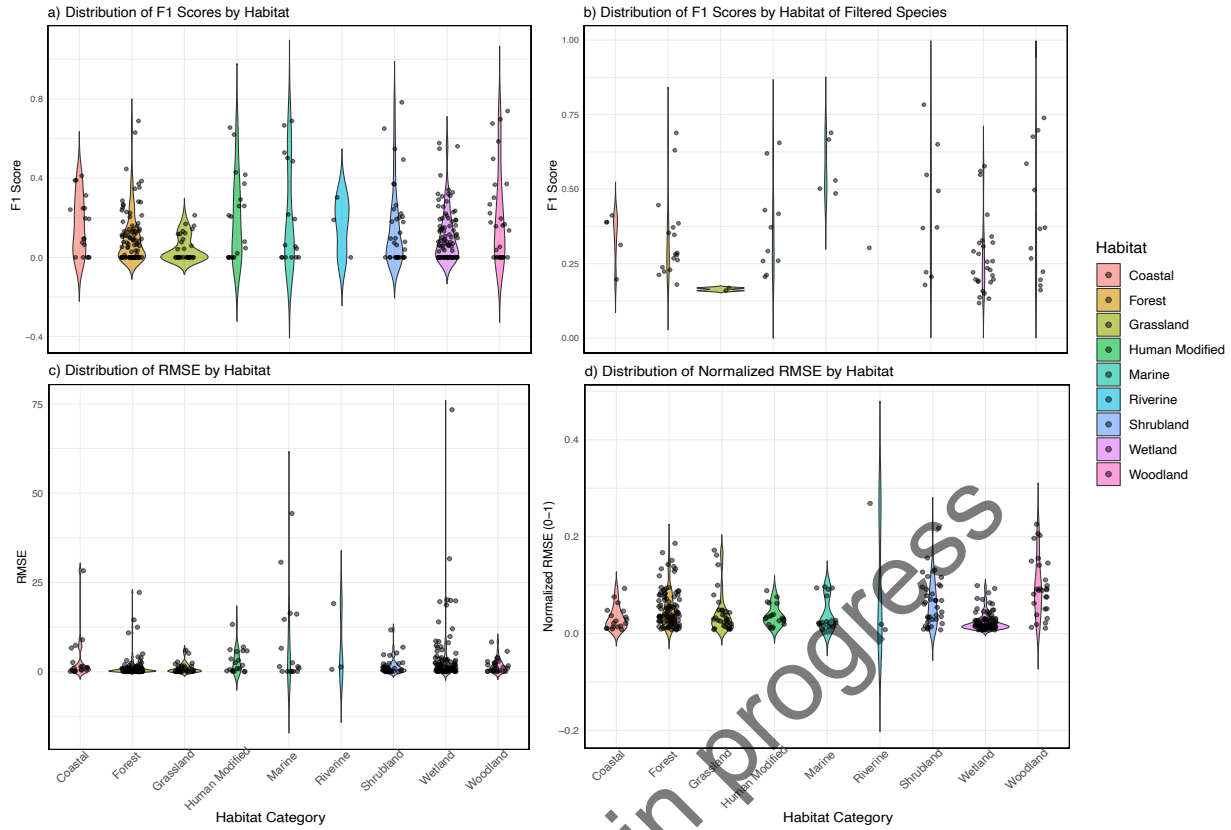


Fig. 8. Distribution of classification performance (F1 score) and regression performance (RMSE) by the preferred habitats of species

5

10

15

20



Fig. S9.

Boundaries for simulated Mean High Water and Salt Marsh Productivity of the two bay reserves
(Grand Bay and Weeks Bay)

5

10

15

20

25

Table. S1. Species abundance maps for additional bird species not listed in the Main Text.
 From the historical scenario (left column) to the SLR scenario (right column). Many species (301 out of 350 species) maps are limited to areas with sufficient observations; coverage may not extend across the entire study region.

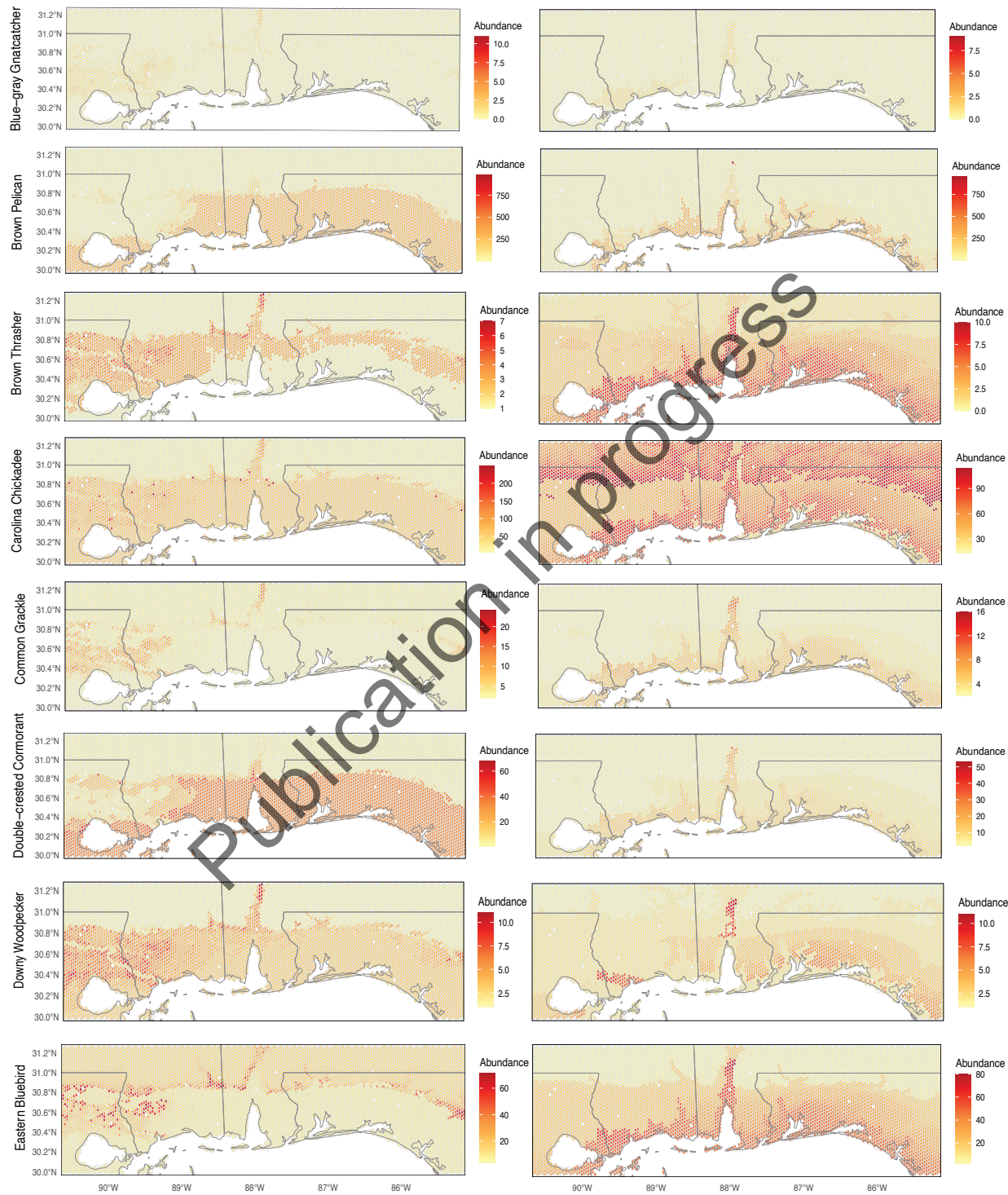


Table. S1. Species abundance maps for additional bird species not listed in the Main Text. - Continued

From the historical scenario (left column) to the SLR scenario (right column)

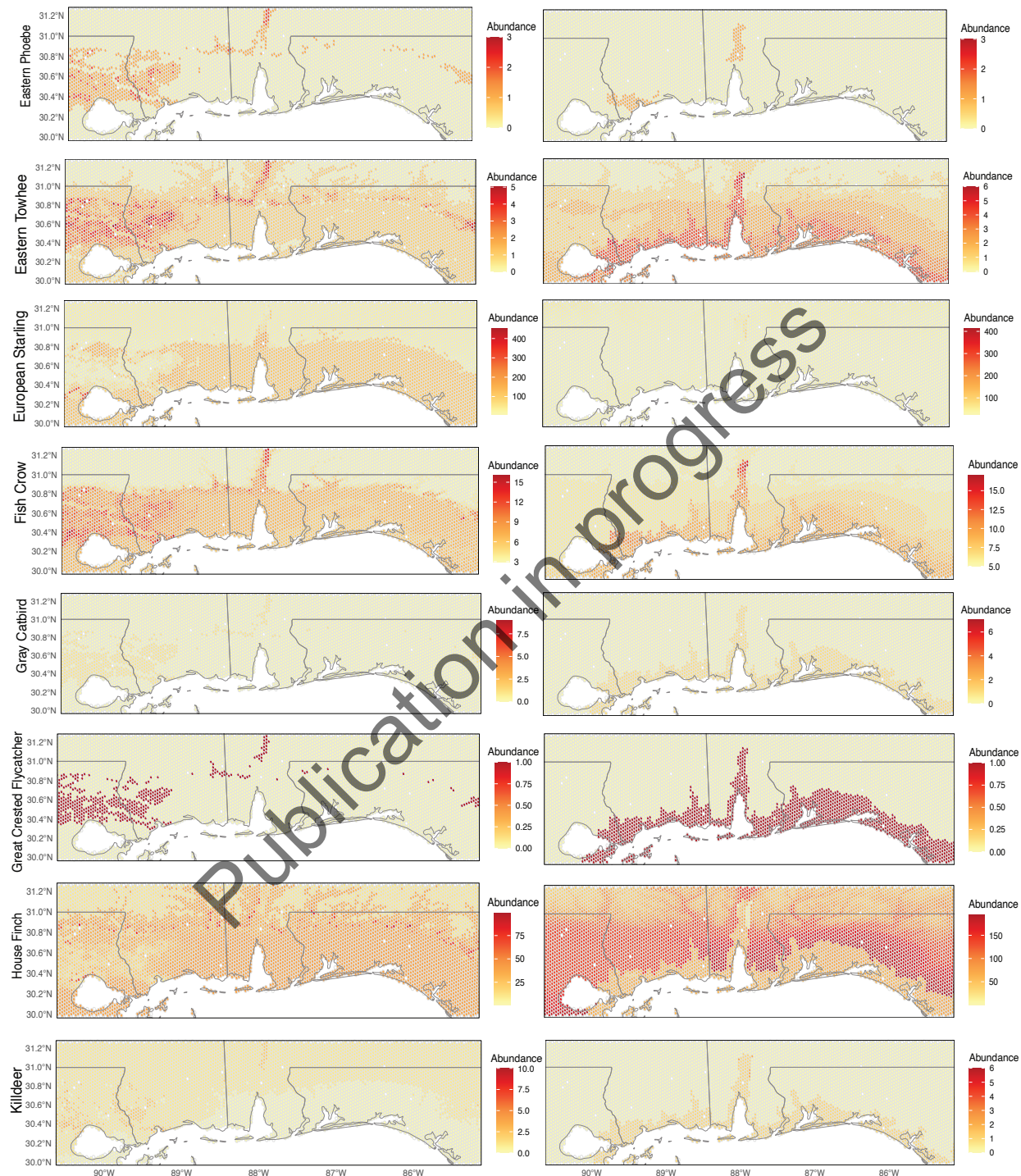
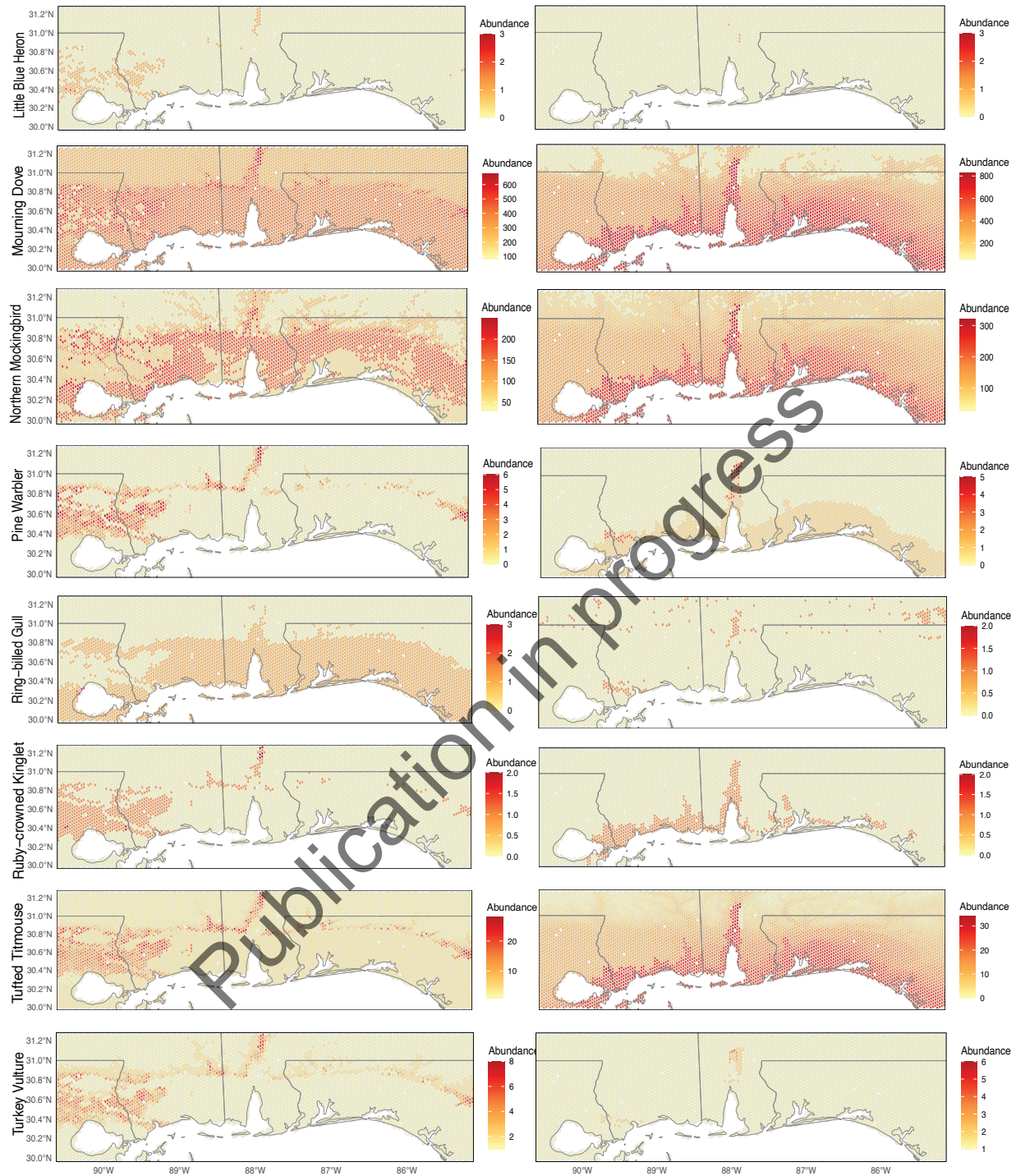
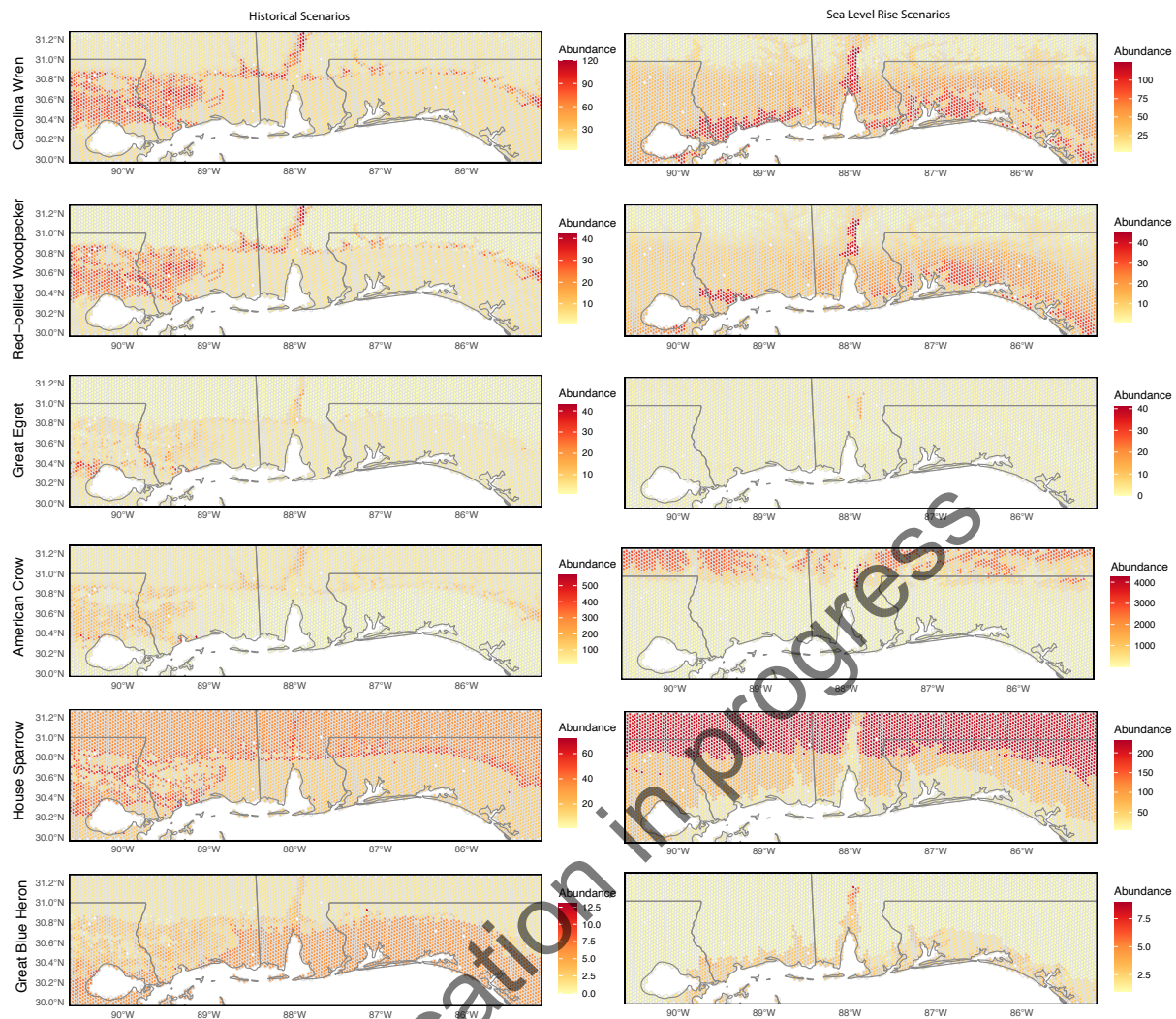


Table. S1. Species abundance maps for additional bird species not listed in the Main Text- continued

From the historical scenario (left column) to the SLR scenario (right column)





5

10

15

References

- Adams, N., Dias, T., Skeen, H. R., Pegan, T., Willard, D. E., Winger, B., Ruegg, K., Weeks, B. C., & Bay, R. (2025). Genetic and morphological shifts associated with climate change in a migratory bird. *BMC Biology*, 23(1), 3. <https://doi.org/10.1186/s12915-024-02107-5>
- Alizad, K., Hagen, S. C., Morris, J. T., Bacopoulos, P., Bilskie, M. V., Weishampel, J. F., & Medeiros, S. C. (2016). A coupled, two-dimensional hydrodynamic-marsh model with biological feedback. *Ecological Modelling*, 327, 29–43. <https://doi.org/10.1016/J.ECOLMODEL.2016.01.013>
- Amatulli, G., Domisch, S., Tuanmu, M. N., Parmentier, B., Ranipeta, A., Malczyk, J., & Jetz, W. (2018). Data Descriptor: A suite of global, cross-scale topographic variables for environmental and biodiversity modeling. *Scientific Data*, 5, 1–15. <https://doi.org/10.1038/sdata.2018.40>
- Bai, J., Kong, S., & Gomes, C. (2020). *Disentangled Variational Autoencoder based Multi-Label Classification with Covariance-Aware Multivariate Probit Model*. <https://doi.org/10.24963/ijcai.2020/595>
- Bai, J., Kong, S., & Gomes, C. P. (2021). *Gaussian Mixture Variational Autoencoder with Contrastive Learning for Multi-Label Classification*. <http://arxiv.org/abs/2112.00976>
- Bishop, C. M. (2016). *Pattern Recognition and Machine Learning | SpringerLink* (1st ed.). Springer New York, NY. <https://link.springer.com/book/9780387310732>
- Bolnick, D. I., Amarasekare, P., Araújo, M. S., Bürger, R., Levine, J. M., Novak, M., Rudolf V. H., Schreiber, S. J., Urban, M. C., & Vasseur, D. (2011). Why intraspecific trait variation matters in community ecology. In *Trends Ecol Evol* (Vol. 26, Issue 4).
- Cameron, A. C., & Trivedi, P. K. (2013). *Regression Analysis of Count Data*. Cambridge University Press. <https://doi.org/10.1017/CBO9781139013567>
- Carmona, C. P., de Bello, F., Mason, N. W. H., & Lepš, J. (2019). Trait probability density (TPD): measuring functional diversity across scales based on TPD with R. *Ecology*, 100(12). <https://doi.org/10.1002/ecy.2876>
- Chen, D., Xue, Y., Chen, S., Fink, D., & Gomes, C. (2016). *Deep Multi-Species Embedding*. <https://doi.org/https://doi.org/10.48550/arXiv.1609.09353>
- Delestrade, A. (2001). Sexual Size Dimorphism and Positive Assortative Mating in Alpine Choughs (*Pyrrhocorax graculus*). *The Auk*, 118(2), 553–556. <https://doi.org/10.1093/auk/118.2.553>
- Dinnage, R. (2024). *NicheFlow: Towards a foundation model for Species Distribution Modelling*. <https://doi.org/10.1101/2024.10.15.618541>
- Falcon, W. (2019). *The PyTorch Lightning team* (PyTorch lightning, 10).
- Huffer, F. W., Sethuraman, J., & Sethuraman, S. (2008). *A study of counts of Bernoulli strings via conditional Poisson processes*. <http://arxiv.org/abs/0801.2115>
- Khosla, P., Teterwak, P., Wang, C., Sarna, A., Tian, Y., Isola, P., Maschinot, A., Liu, C., & Krishnan, D. (2021). *Supervised Contrastive Learning*. <http://arxiv.org/abs/2004.11362>
- Kingma, D. P., & Welling, M. (2022). *Auto-Encoding Variational Bayes*. <http://arxiv.org/abs/1312.6114>
- Kong, S., Bai, J., Lee, J. H., Chen, D., Allyn, A., Stuart, M., Pinsky, M., Mills, K., & Gomes, C. P. (2020). *Deep Hurdle Networks for Zero-Inflated Multi-Target Regression: Application to Multiple Species Abundance Estimation*. <http://arxiv.org/abs/2010.16040>
- Li, L., Cole, S., Rodriguez-Flores, J. M., Hestir, E., Fink, D., Viers, J. H., Medellin-Azuara, J., Conklin, M., & Harmon, T. (2025). Synergies Between Agricultural Production and Shorebird Conservation With Climate Change in the Central Valley, California, With Optimized Water Allocation and Multi-Benefit Land Use. *Global Change Biology*, 31(6). <https://doi.org/10.1111/gcb.70304>
- Marcy, D., Herold, N., Waters, K., Brooks, W., Hadley, B., Pendleton, M., & Schmid, K. (2011). *New Mapping Tool and Techniques For Visualizing Sea Level Rise And Coastal Flooding Impacts National Oceanic and Atmospheric Administration (NOAA) Coastal Services Center*. www.csc.noaa.gov
- NCOOS. (2017). *Predicting Impacts of Sea Level Rise in the Northern Gulf of Mexico - NCCOS - National Centers for Coastal Ocean Science*. <https://coastalscience.noaa.gov/project/predicting-impacts-sea-level-rise-gulf-mexico/>
- NOAA. (2024). *Coastal Change Analysis Program Regional Land Cover*. Charleston: SC: NOAA Office for Coastal Management. <https://coast.noaa.gov/digitalcoast/data/ccapregional.html>
- NOAA National Geophysical Data Center. (2010). *Northern Gulf 1 arc-second MHW Coast Digital Elevation Model*. NOAA National Centers for Environmental Information.
- Parris, A. S., Bromirski, P., Burkett, V., Cayan, D. R., Culver, M. E. 1963-, Hall, J., Horton, R. M., Knuuti, K., Moss, R. H., Obeysekera, J., Sallenger, A. H., & Weiss, J. (2012). *Global sea level rise scenarios for the United States National Climate Assessment*. <http://view/noaa/11124>
- R core team. (2021). *The R Project for Statistical Computing*. <https://www.r-project.org/>

- Sullivan, B., C. Wood, M. J. Iliff, R.E. Bonney, D. Fink, & S. Kelling. (2009). eBird: a citizen-based bird observation network in the biological sciences. *Biological Conservation*, 142:2282–2292.
- Tobias, J. A., Sheard, C., Pigot, A. L., Devenish, A. J. M., Yang, J., Sayol, F., Neate-Clegg, M. H. C., Alioravainen, N., Weeks, T. L., Barber, R. A., Walkden, P. A., MacGregor, H. E. A., Jones, S. E. I., Vincent, C., Phillips, A. G., Marples, N. M., Montaño-Centellas, F. A., Leandro-Silva, V., Claramunt, S., ... Schleuning, M. (2022a). AVONET: morphological, ecological and geographical data for all birds. *Ecology Letters*, 25(3), 581–597. <https://doi.org/10.1111/ele.13898>
- Tobias, J. A., Sheard, C., Pigot, A. L., Devenish, A. J. M., Yang, J., Sayol, F., Neate-Clegg, M. H. C., Alioravainen, N., Weeks, T. L., Barber, R. A., Walkden, P. A., MacGregor, H. E. A., Jones, S. E. I., Vincent, C., Phillips, A. G., Marples, N. M., Montaño-Centellas, F. A., Leandro-Silva, V., Claramunt, S., ... Schleuning, M. (2022b). AVONET: morphological, ecological and geographical data for all birds. *Ecology Letters*, 25(3), 581–597. <https://doi.org/10.1111/ele.13898>
- Weeks, B. C., Naeem, S., Winger, B. M., & Cracraft, J. (2020). The relationship between morphology and behavior in mixed-species flocks of island birds. *Ecology and Evolution*, 10(19), 10593–10606. <https://doi.org/10.1002/ece3.6714>
- Yan, Y., Shao, B., & Davis, C. C. (2024). *A generative deep learning approach for global species distribution prediction*. <https://doi.org/10.1101/2024.12.10.627845>